MASTER COPY KEEP THIS COPY FOR REPRODUCTION PURPOSES

REPORT DOCUMENTATION PAGE

Form Approved
OMB No. 0704-0188

1. AGENCY USE ONLY (Leave blank)	2. REPORT DATE	3. REPORT TYPE AND DATES COVERED
	7 March 1994	Final 7/15/91-7/14/94

4. TITLE AND SUBTITLE
Fractal Aggregate Random Media Analysis and Applications

5. FUNDING NUMBERS
DAAL03-91-G-0229

6. AUTHOR(S)
Kung-Hau Ding

7. PERFORMING ORGANIZATION NAME(S) AND ADDRESS(ES)
Regents of New Mexico State University
Physical Science Laboratory
P.O. Box 30002
Las Cruces, NM 88003-0002

8. PERFORMING ORGANIZATION REPORT NUMBER
N/A

9. SPONSORING / MONITORING AGENCY NAME(S) AND ADDRESS(ES)
U. S. Army Research Office
P. O. Box 12211
Research Triangle Park, NC 27709-2211

10. SPONSORING / MONITORING AGENCY REPORT NUMBER
ARO 29107.1-GS-SAH

11. SUPPLEMENTARY NOTES
The view, opinions and/or findings contained in this report are those of the author(s) and should not be construed as an official Department of the Army position, policy, or decision, unless so designated by other documentation.

12a. DISTRIBUTION / AVAILABILITY STATEMENT
Approved for public release; distribution unlimited

12b. DISTRIBUTION CODE

13. ABSTRACT (Maximum 200 words)

The research performed during the period of July 1991 – September 1993 was focused on the theoretical formulations and numerical simulations of electromagnetic wave interaction with random fractal clusters and electromagnetic wave propagation and scattering in media with adhesive scatterers, and their applications in atmospheric aerosols and random media consisting of aggregated particles. The major accomplishments in this period include: (i) Development of a fractal-based aggregated model and a rigorous T-matrix approach for studying the light scattering and absorption by agglomerated particles. We have simulated the structure of random clusters, determine the fractal dimension, and investigated their

 (continued on reverse side)

14. SUBJECT TERMS	15. NUMBER OF PAGES
	39
	16. PRICE CODE

17. SECURITY CLASSIFICATION OF REPORT	18. SECURITY CLASSIFICATION	19. SECURITY CLASSIFICATION OF ABSTRACT	20. LIMITATION OF ABSTRACT
UNCLASSIFIED	UNCLASSIFIED	UNCLASSIFIED	UL

optical properties. (ii) Development of a sticky particle model for simulating a random medium consisting of aggregated particles. We have studied the propagation and scattering of waves in such random media and performed computer simulations to determine the cluster size distribution and the fractal dimension for agglomerates. In the following, we describe these major accomplishments.

Fractal Aggregate Random Media Analysis and Applications

Final Report

Principal Investigator

Kung-Hau Ding

U.S. Army Research Office

Grant: DAAL03-91-G-0229

Physical Science Laboratory

New Mexico State University

Box 30002

Las Cruces, New Mexico 88003-0002

1. STATEMENT OF RESEARCH PROBLEM

The aerosols in atmosphere are often random cluster of small primary particles with ramified appearance. They are considered to be fractal aggregates with a noninteger dimensions and they have the important property of invariance under scale transformation. This essential fractal morphology has already been demonstrated for soot and smoke. In this research we investigate the scattering and absorption properties of aggregated aerosol particles based on a fractal cluster model. A rigorous treatment of the scattering of electromagnetic radiations is pursued to take into account the features of inter-connected primary particles. Specific research efforts include using the T-matrix method together with the translation addition theorem for vector spherical waves to solve the scattering and absorption by connected spherules with clustering and branched structures; computer simulating the configurations for random aggregates, solving the scattering and absorption cross sections for random agglomerates; calculating the average optical properties of random clusters over configurations; and validating the theoretical model by comparison with experimental measurements.

2. SUMMARY OF RESULTS

The research performed during the period of July 1991 – September 1993 was focused on the theoretical formulations and numerical simulations of electromagnetic wave interaction with random fractal clusters and electromagnetic wave propagation and scattering in media with adhesive scatterers, and their applications in atmospheric aerosols and random media consisting of aggregated particles. The major accomplishments in this period include: (i) Development of a fractal-based aggregated model and a rigorous T-matrix approach for studying the light scattering and absorption by agglomerated particles. We have simulated the structure of random clusters, determine the fractal dimension, and investigated their optical properties. (ii) Development of a sticky particle model for simulating a random medium consisting of aggregated particles. We have studied the propagation and scattering of waves in such random media and performed computer simulations to determine the cluster size distribution and the fractal dimension for agglomerates. In the following, we describe these major accomplishments.

2.1 Light Scattering and Absorption by Agglomerated Particles

The aerosols in atmosphere are often random clusters of small primary particles with ramified and connected appearance. They are considered to be fractal aggregates and the essential fractal morphology has already been demonstrated for soot and smoke [1-4]. The aggregation process of small primary particles has been simulated by applying the cluster-cluster aggregation (CCA) algorithm [5-10]. In this model, the primary particles undergo random walk simultaneously to form small clusters initially, and subsequent collisions will lead to their aggregation. The fractal dimensions of resultant agglomerates are determined by finding out the power form relationship between the number of primary particles and the cluster gyration radius [9-10]. To study the scattering and absorption of electromagnetic waves by such fractal aggregates, a T-matrix approach together with the translation addition theorem for vector spherical waves is employed to solve the aggregate scattering problem [11-12]. Numerical results for the phase function, scattering and absorption cross sections are illustrated as a function of observation angles, cluster structures, particle sizes and number of primary particles. The model predicted that the effects of multiple scattering may cause scattering and absorption cross sections of an aggregate that will initially increase with its size (number of primary particles or size of

monomer), then saturate and decrease when its size further increase. We also made the comparison with the measurements of extinction cross sections on soot particles over the wavelength region from millimeter wave to infrared [13]. It is shown that the extinction decreases linearly with increasing wavelength, however, the slope is not in agreement with the measurements.

2.1.1 Multiple Scattering Formulation

Consider a plane wave incident on an aggregate in the direction of $\hat{k}_i$, $\hat{k}_i = \sin\theta_i \cos\phi_i \hat{x} + \sin\theta_i \sin\phi_i \hat{y} + \cos\theta_i \hat{z}$. The aggregate is modeled as a cluster of N connected identical spheres centered at $\bar{r}_1$, $\bar{r}_2$, ..., $\bar{r}_N$, each of which has radius a and refractive index μ_s. The background medium has the refractive index μ. In a cluster of N particles, the total amount of wave excitation exerted on the particle ℓ is the sum of incident field and scattered fields from the other particles,

$$\bar{w}^{(\ell)} = \sum_{j \neq \ell}^{N} \bar{\bar{\sigma}}(k\bar{r}_\ell \bar{r}_j) \cdot \bar{\bar{T}}^{(j)} \cdot \bar{w}^{(j)}(\bar{r}) + e^{i\bar{k}_i \cdot \bar{r}_\ell} \ \bar{a}^{inc} \tag{1}$$

where $\bar{w}^{(\ell)}$ and $\bar{a}^{inc}$ are column vectors that represent the exciting field of the scatterer ℓ and the incident field respectively, $\bar{\bar{T}}^{(j)}$ is the T matrix that describes scattering from the scatterer j, $\bar{\bar{\sigma}}(\bar{r}_\ell \bar{r}_j)$ is the transformation matrix used to convert spherical waves centered at $\bar{r}_j$ to spherical waves centered at $\bar{r}_\ell$ (see Appendix A), and k is the wave number of the background medium [12].

The multiply scattered field $\bar{a}^{s(\ell)}$ of particle ℓ is given as

$$\bar{a}^{s(\ell)} = \bar{\bar{T}}^{(\ell)} \cdot \bar{w}^{(\ell)} \tag{2}$$

where $\bar{a}^{s(\ell)}$ is the column vector that represent the scattered field from the particle ℓ. The total scattered field at a field point $\bar{r}$ is given by the summation of scattered waves from all particles

$$\bar{E}^s(\bar{r}) = \sum_{\ell=1}^{N} \sum_{m,n} \left[a_{mn}^{s(M)(\ell)} \bar{M}_{mn}(k\bar{r}\bar{r}_\ell) + a_{mn}^{s(N)(\ell)} \bar{N}_{mn}(k\bar{r}\bar{r}_\ell) \right] \tag{3}$$

where $\bar{M}_{mn}$ and $\bar{N}_{mn}$ are vector spherical waves (see Appendix B) [12], and $a_{mn}^{s(M)(\ell)}$ and $a_{mn}^{s(N)(\ell)}$ are expansion coefficients for the scattered field form particle ℓ. The far scattered field in the direction $\hat{k}_s$, $\hat{k}_s = \sin\theta_s \cos\phi_s \hat{x} + \sin\theta_s \sin\phi_s \hat{y} + \cos\theta_s \hat{z}$, can be expressed as

$$\bar{E}^s = \frac{e^{ikr}}{kr} \left(\hat{v}_s E_{vs} + \hat{h}_s E_{hs} \right) \tag{4}$$

with $\hat{v}_s = \cos\theta_s \cos\phi_s \hat{x} + \cos\theta_s \sin\phi_s \hat{y} - \sin\theta_s \hat{z}$ and $\hat{h}_s = -\sin\phi_s \hat{x} + \cos\phi_s \hat{y}$ being the vertical and horizontal polarization vectors respectively for the scattered wave. From (3) and (4), E_{vs} and E_{hs} can be expressed as

$$E_{vs} = \sum_{m,n} \gamma_{mn} i^{-n-1} \left[a_{mn}^{s(M)} \hat{v}_s \cdot \overline{C}_{mn}(\theta_s, \phi_s) + i a_{mn}^{s(N)} \hat{v} \cdot \overline{B}_{mn}(\theta_s, \phi_s) \right] \tag{5}$$

$$E_{hs} = \sum_{m,n} \gamma_{mn} i^{-n-1} \left[a_{mn}^{s(M)} \hat{h}_s \cdot \overline{C}_{mn}(\theta_s, \phi_s) + i a_{mn}^{s(N)} \hat{h} \cdot \overline{B}_{mn}(\theta_s, \phi_s) \right] \tag{6}$$

where $\overline{B}_{mn}$ and $\overline{C}_{mn}$ are vector spherical harmonics [12], γ_{mn} are coefficients as defined in Appendix B, and

$$a_{mn}^{s(M)} = \sum_{\ell=1}^{N} e^{-i\bar{k}_s \cdot \bar{r}_\ell} a_{mn}^{s(M)(\ell)} \tag{7}$$

$$a_{mn}^{s(N)} = \sum_{\ell=1}^{N} e^{-i\bar{k}_s \cdot \bar{r}_\ell} a_{mn}^{s(N)(\ell)} \tag{8}$$

Instead of solving the exciting field coefficients, we can combine equations (1) and (2) to form equations for the scattered field coefficients

$$\overline{a}^{s(\ell)} = \sum_{j \neq \ell}^{N} \overline{\overline{T}}^{(\ell)} \cdot \overline{\overline{\sigma}}(k\overline{r_\ell r_j}) \cdot \overline{a}^{s(j)} + e^{i\bar{k}_i \cdot \bar{r}_\ell} \ \overline{\overline{T}}^{(\ell)} \cdot \overline{a}^{inc} \tag{9}$$

Thus the multiple scattering solution consists of solving (9) numerically for $\overline{a}^{s(\ell)}$ and then using (3) to calculate the scattered field $\overline{E}^s(\bar{r})$.

Equation (9) is solved by using an iterative scheme [14]. The result for the $(\nu+1)$ iteration is

$$\overline{a}^{s(\ell)(\nu+1)} = e^{i\bar{k}_i \cdot \bar{r}_\ell} \ \overline{\overline{T}}^{(\ell)} \cdot \overline{a}^{inc} + \sum_{j \neq \ell}^{N} \overline{\overline{T}}^{(\ell)} \cdot \overline{\overline{\sigma}}(k\overline{r_\ell r_j}) \cdot \overline{a}^{s(j)(\nu)} \tag{10}$$

where ν denotes the νth iterated solution. The initial solution of $\overline{a}^{s(\ell)(1)}$ is just the first term on the right-hand side of (10). The physical correspondence is the first-order scattering, the second-order scattering, and so on.

The bistatic scattering cross section is defined by

$$\sigma_{\beta\alpha}(\theta_s, \phi_s; \theta_i, \phi_i) = 4\pi \lim_{r \to \infty} r^2 \frac{|E_{\beta s}|^2}{|\overline{E}_\alpha^{inc}|^2} \tag{11}$$

where α and β represent the polarization states of the incident and scattered wave respectively, and α and β can be v or h.

2.1.2 Generation of Random Aggregates

Aggregation is an irreversible growth process in which initially dispersed primary particles collide and stick together to build the clumping structure. For example, soot particles are formed by random collision of small carbon spheres in the turbulent region of a flame. Growth models such as diffusion-limited aggregation (DLA) [5] and cluster-cluster aggregation (CCA) [6] have been applied to obtain information about the growth processes and predict the fractal structure of aggregates. In the DLA model primary particles are added to a growing cluster successively. Each new particle moves in a random manner, its path being chosen by the Monte Carlo method. The CCA model is a variation of the DLA model, in which many particles undergoing random walk simultaneously to form small clusters initially, and subsequent collisions will lead to their aggregation. However, many studies of soot particles have shown that they are formed by cluster-cluster aggregation [5-7] with an open structure and the fractal dimensions are in the range of $1.7 - 1.9$.

The mechanism used here for generating fractal clusters is the hierarchical cluster-cluster aggregation algorithm [8]. In this model collisions are restricted to clusters of the same size during the simulation, where dimers collide and stick to form tetramers, tetramers collide and stick to make octamers, etc. This simulation process is more speedy than the CCA model and produces clusters of very similar fractal dimensions [8]. Examples of 3-dimensional aggregates obtained by this process are illustrated in Figure 1.

For fractal clusters, despite their random appearance, there exists a power form relationship between the number of primary spheres N and the radius of gyration R_g

$$N = cR_g^{D_f} \tag{12}$$

where D_f is the fractal dimension and c is a proportionality constant. Assuming all primary spheres to have equal mass, the radius of gyration of an aggregate is given by

$$R_g^2 = \frac{1}{N}\sum_{i=1}^{N} r_i^2 \tag{13}$$

where r_i is the distance from the monomer i to the center of aggregate. The fractal dimension $D_f \approx 1.74$ is deduced from the $\ln(N)$–$\ln(R_g)$ data curve fitting in Figure 2.

2.1.3 Simulation Results

In this section we simulate the scattering of optical waves by soot aggregates that are generated from the hierarchical CCA model with $ka = 0.05$ and $ka = 0.25$. A typical refractive index for soot particle $\mu_s = 1.75 + i0.5$ is considered in the simulation.

Assuming $\hat{k}_i = \hat{x}$, we calculate the bistatic scattering coefficients as a function of scattering angles. For Figures 3(a) and 3(b), we consider the scattering by a cluster of $N = 32$ primary spheres with $ka = 0.05$ and $ka = 0.25$, respectively. We plot bistatic scattering coefficients as a function of ϕ_s with $\theta_s = 90°$. The coefficients show that a maximum scattering is in the forward direction and the result for vv is larger than that for hh. There is a minimum for hh around $\phi_s = 90°$ because the induced dipoles in small primary spheres are pointing in the same direction as $\hat{k}_s$. In Figures 4(a) and 4(b), we illustrate the case for a larger cluster with $N = 128$ monomers. Figure 4(a) shows that for a larger cluster we have a much stronger forward scattering than that in Figure 3. The minima around 90° for the hh are also due to the induced dipoles' orientations.

In Figure 5, we plot the ratio of $\frac{\sigma_s^{(N)}}{N\sigma_s^{(1)}}$ as a function of the number of primary particles in a cluster. $\sigma_s^{(N)}$ is the scattering cross section for an agglomerate with N number of monomers. $\sigma_s^{(1)}$ is the scattering cross section for a primary particle. The results have been averaged over 30 realizations. It shows that the scattering increases with N when clusters are small (small N or small ka). However, the multiple scattering becomes important as clusters grow larger which is indicated by the saturation of scattering cross section. The ratio of $\frac{\sigma_a^{(N)}}{N\sigma_a^{(1)}}$ is shown in Figure 6, where the subscript a is used to denote the absorption cross section. As expected, the absorption increases with N when multiple scattering is a minor effect. However, when the agglomerates become larger, the multiple scattering effects will block the absorption for the inner particles within the aggregates. In Figure 7, we illustrate the results for extinction cross section which is equal to the sum of scattering and absorption cross sections $\sigma_e = \sigma_s + \sigma_a$.

Figure 8 shows the wavelength dependence of extinction cross section per constituent particle. The index of refraction for carbon as a function of frequency is obtained from [15]. It is shown that the extinction decreases linearly with increasing wavelength, but the slope is not in agreement with the experimental measurements [13]. However, in the above work we have assumed only dipole interaction between primary particles and they touching only at one point on the surface. This assumption has been justified for dielectric particles, because in this case the displacement current dominates over the conduction current. In

soot particles, the carbon monomers may overlap by nucleation and may have very high conductivity. For these cases, we may need to include more multipole moments in the T-matrix calculation to take into account the higher order interaction between primary particles. Also, the sphere model may not be an accurate one for highly absorptive cases. This is due to the difficulty of field penetration into the sphere.

2.2 Scattering of Waves in Media with Adhesive Particles

Some terrain media (e.g. snow, ice) may consists of aggregated particles, also they can be characterized as dense media. In a dense medium, the inhomogeneities occupy an appreciable volume fraction, the classical assumption of independent scattering is not valid, we have to consider the effects of correlated scattering and mutual coherent wave interactions among scatterers. However, the aerosol can be characterized as locally dense medium because of the primary particles being aggregated together within a cluster. In order to account for the clustering of particles, we have applied the sticky hard sphere (SHS) model [16] by introducing a surface adhesive force between two particles. The analytic wave approaches, quasicrystalline approximation (QCA) and quasicrystalline approximation with coherent potential (QCA-CP) [12], which take into account the mutual coherent wave interactions, were applied to derive closed-form equations for effective propagation constants in random media with sticky particles. The model produced results that explain the observed features of the laboratory experiment [17]. The experiment involved light scattering from colloidal silica particles suspended in a solvent background. The comparison with theory shows that the experimental data can be explained by assuming the silica particles have some adhesion, but cannot explained without this assumption. The sticky particle pair distribution function has been used by other researchers to explain x-ray scattering from aggregated gold colloids [18]. We also performed Monte Carlo simulations to generate random media with aggregated particles. The computer simulated random aggregated media has been shown to have fractal structure, and the fractal dimension depends on the concentration and stickiness of particles.

2.2.1 Pair Distribution Function for Media with Sticky Particles

We shall consider a system consisting of non-interpenetrable, spherical particles of diameter d with a non-zero surface adhesive force, *i.e.* sticky hard spheres (SHS). In

this model, the interaction between two particles is of very short range, the interparticle potential $u(r)$ is described by [16]:

$$u(r) = \lim_{s \to d} \begin{cases} \infty & \text{for } 0 < r < s \\ \ln \frac{12\tau(d-s)}{d} & \text{for } s < r < d \\ 0 & \text{for } r > d \end{cases} \tag{14}$$

where the limit is taken in such a way that the relation

$$\lim_{s \to d}(d-s)e^{-u(r)} = \frac{d}{12\tau} < \infty \tag{15}$$

holds with d and τ being held fixed. The parameter τ in (14) is dimensionless, and its inverse is a measure of the attraction or stickiness between particles. The case of $\tau^{-1} = \infty$ corresponds to infinite stickiness and $\tau^{-1} = 0$ corresponds to non-sticky particles.

The pair distribution function $g(r)$ measures the probability of finding a particle at a point r given a particle at $r = 0$. The total correlation function $h(r)$ between a pair of particles is defined as

$$h(r) = g(r) - 1 \tag{16}$$

The direct correlation function $c(r)$ between a pair of particles, which is short-ranged, is related to $h(r)$ by means of the Ornstein–Zernike relation:

$$h(r) = c(r) + n \int d\vec{r}' \, c(r') \, h(|\vec{r} - \vec{r}'|) \tag{17}$$

where n is the number of particles per unit volume. Equation (17) indicates that the total influence of a particle on another particle in the presence of remaining particles can be decomposed into a sum of the direct effect and the indirect effect through other particles.

Under the Percus–Yevick (PY) approximation [19], correlation functions $c(r)$ and $h(r)$ are approximated by

$$c(r) = 0 \qquad \text{for } r > d \tag{18}$$

$$h(r) = -1 + \frac{td}{12\tau}\delta(r-d) \qquad \text{for } 0 < r < d \tag{19}$$

respectively, with t a dimensionless parameter to be determined later. The parameter t tends to zero in the limit $\tau^{-1} = 0$. The PY approximation of the pair distribution function $g(r)$ for the sticky spherical particles can be solved analytically using the factorization method of Baxter [20].

The Ornstein–Zernike relationship (17) can be Fourier transformed to obtain a convenient algebraic equation:

$$1 - n\tilde{C}(p) = \left\{1 + n\tilde{H}(p)\right\}^{-1} \tag{20}$$

where $\tilde{H}(\bar{p})$ and $\tilde{C}(\bar{p})$ are the three dimensional Fourier transform of $h(\bar{r})$ and $c(\bar{r})$. According to the Wiener–Hopf technique due to Baxter [20], the left-hand side of (20) can be factorized into the form

$$1 - n\tilde{C}(p) = \tilde{Q}(p)\tilde{Q}(-p) \tag{21}$$

where $\tilde{Q}(p)$ is defined by

$$\tilde{Q}(p) = 1 - 2\pi n \int_0^d dr\, e^{ipr} Q(r) \tag{22}$$

and $Q(r)$ is a real function, $Q(r)=0$ for $r>d$. For sticky particles, in the range $0<r<d$, $Q(r)$ has a closed-form expression:

$$Q(r) = A\frac{r^2}{2} + Br + D \tag{23}$$

where

$$A = \frac{1 + 2f - \mu}{(1-f)^2} \tag{24}$$

$$B = \frac{(-3f + \mu)d}{2(1-f)^2} \tag{25}$$

$$D = -A\frac{d^2}{2} - Bd + \frac{td^2}{12} \tag{26}$$

$$f = \frac{\pi}{6} n d^3 \tag{27}$$

$$\mu = tf(1-f) \tag{28}$$

For a given volume fraction f and stickiness parameter τ, the parameter t is determined by the quadratic equation [16,21]

$$\frac{f}{12}t^2 - (\tau + \frac{f}{1-f})t + \frac{1 + f/2}{(1-f)^2} = 0 \tag{29}$$

Moreover, a further condition to determine the solution of t is that $\tilde{Q}(0)$ must be positive, or [16,21]

$$\mu < 1 + 2f \tag{30}$$

The procedure for calculating the pair function is as follows. Given the particle diameter d, particle concentration f, and particle stickiness τ, the parameter t is first determined

from (29)–(30). By using the parameter t and equations (23)–(28), $Q(r)$ for $0<r<d$ can be computed. Then the Fourier transform $\tilde{Q}(p)$ is calculated by using (22), and $\tilde{C}(\bar{p})$ is evaluated by using (21). Next, $\tilde{H}(p)$ is computed by solving equation (20). Then $h(r)$ is obtained by taking an inverse Fourier transform from $\tilde{H}(p)$. Finally, the pair distribution function $g(r)$ can be calculated from (16).

In Figure 9, the pair distribution functions are shown for systems with sticky particles of identical size, $\tau=0.2$ and $\tau=0.5$, and compared with the non-sticky case for $f=0.3$. The major features for the pair distribution functions of sticky particles are the occurrence of discontinuities at the particle separation equals one and two diameters. The discontinuity at $r=d$ is because the particles can not interpenetrate each other. The height of the peak at $r=d$ grows rapidly with the increasing of particle stickiness while the width of this peak reduces, which shows a stronger connectedness between particles as particles getting more sticky, and other particles are more likely to be excluded from the region $d<r<2d$. Therefore, in a dense medium with sticky particles, the sticky particles tend to aggregate together. The discontinuity at $r=2d$ arises from the fact that for $r>2d$, physically, when the separation between two particles is larger than twice the diameter, the probability of these two particles bound or connect to a third particle drops to zero. In Figure 10, the pair distribution functions are plotted for $f=0.2$ and $f=0.4$, with stickiness $\tau=0.2$. For higher concentration of sticky particles, the pair distribution function displays more fluctuations just as the case of non-sticky particles.

2.2.2 Monte Carlo Simulation of Media with Sticky Particles

Basically, the Monte Carlo technique used in simulating the clustering of particles is to deposit particles one by one into a box which contains all particles subject to the condition that no overlap between particles is allowed [22]. However, the essence in the simulation process for the case of sticky particles is that we have to calculate, before depositing each trial particle, the probabilities that determine the bound or unbound states for the trial particle. These probabilities depend on the stickiness of particles, the size of particle, and the number of particles existing in the box [23-24]. After selecting a particular bound or unbound state for the trial particle, we will determine its possible position in accordance with the selected bound state according to a uniform probability. Then we test for overlap and reject the trial position when a overlap is detected.

Volume Fraction	0.2	0.2	0.2	0.3	0.3	0.3
Stickiness Parameter	0.2	0.5	1	0.2	0.5	1
Fractal Dimension	1.72	1.74	1.59	1.90	1.76	1.60
Constant c	1.86	1.64	1.73	1.75	1.65	1.84

Table 1: Numerical Results for D_f and c

In Figure 11, the Monte Carlo simulation of the pair distribution function is shown for a system with $N = 512$ sticky particles for the case of $f = 0.3$, and $\tau = 0.2$. It shows that the Monte Carlo simulation also indicates the discontinuity in the pair function when the distance equals two diameters. Generally, the result shows a good agreement with the Percus-Yevick approximation. A typical realization of the simulated medium with sticky particles is shown in Figure 12. Clearly, we can see that particles form aggregates and the structure of the cluster is quite open. The fractal dimensions of these agglomerates can be calculated from the power-law relationship between the radius of gyration of a cluster and the number of particles in a cluster as discussed in Section 2.1.2. The fractal dimension depends on the concentration of particles and the stickiness of particles. Based on our simulations, for 512 particles and 30 realizations, the computed fractal dimension is less than 2 and larger than 1.7 as illustrated shown in Figure 13 and Table 1.

2.2.3 Computation of Effective Propagation Constant

When the scatterers in a medium are close to each other, it is important to consider the mutual coherent wave interactions between scatterers and the effects of correlated scattering. For many years we have used analytic wave theory and approximations, such as quasi-crystalline approximation (QCA) and quasi-crystalline approximation with coherent potential (QCA-CP), to study the electromagnetic wave propagation and scattering in uniformly dense media [12,25-27]. In these two approaches, the mutual coherent wave interactions among particles are weighted by the pair distribution functions. We have also applied Monte Carlo method to directly solve the Foldy-Lax multiple scattering equations for media with densely distributed particles. The results of Monte Carlo simulations agree very well with those of QCA and QCA-CP [14], which is also confirmed by using the recursive T-matrix numerical algorithm [28]. Also, controlled laboratory experiments

have verified the QCA and QCA-CP theories [29]. The important advantage of using these two analytic approximations is that, since they start with Maxwell's equations, the effects of correlated scattering from different scatterers, the mutual coherent wave interactions between scatterers, and spatial correlation among particles are all included in their analytic formulations. Moreover, to solve the scattering problem in a random medium using these two analytic approaches, we only need to solve the integral equation of the average field once, which is computationally much more efficient than the Monte Carlo approach which needs to solve integral equations for many realizations.

In this section, the effective propagation constants for QCA and QCA-CP are given, and the solution with the sticky particle pair function are illustrated. The dispersion relationships for QCA and QCA-CP are given as [12,25-27]:

$$K^2 = k^2 + \frac{f(k_s^2 - k^2)}{1 + \frac{k_s^2 - k^2}{3k^2}(1-f)} \left\{ 1 + i \frac{2(k_s^2 - k^2)ka^3(1-f)^4}{9\left[1 + \frac{k_s^2 - k^2}{3k^2}(1-f)\right][1 + 2f - tf(1-f)]^2} \right\} \tag{31}$$

$$K^2 = k^2 + \frac{f(k_s^2 - k^2)}{1 + \frac{k_s^2 - k^2}{3K^2}(1-f)} \left\{ 1 + i \frac{2(k_s^2 - k^2)Ka^3(1-f)^4}{9\left[1 + \frac{k_s^2 - k^2}{3K^2}(1-f)\right][1 + 2f - tf(1-f)]^2} \right\} \tag{32}$$

respectively, where K is the effective propagation constant, f is the fractional volume of particle, k_s is the wave number inside the particle, k is the wave number of background medium, a is the radius of particle, and t is the parameter in term of stickiness τ determined form equation (29).

The attenuation rates ($2\mathrm{Im}(K)$) for various values of stickiness parameter τ as a function of fractional volume are shown in Figure 14. It can be seen that the sticky model predicts larger attenuation for all fractional volumes than the non-sticky model. We also note that the maximum attenuation shifts with stickiness which indicates the scattering by effectively larger particles formed by the clustering. At a value of $\tau = 0.2$, the predicted scattering may be greater than the independent scattering.

The concept of sticky particles has been explored by Penders and Vrij in an interpretation of turbidity (attenuation of a light beam by scattering when passing through a sample) studies on colloidal silica particles [17]. Details of the experimental procedure are given in Jansen *et. al.* [30]. In these experiments, results from light scattering off of high concentrations of silica particles is explained with the sticky particle pair function described in section 2.2.1.

Particle Solvent	SE2 toluene	SJ9 toluene	SJ4 benzene
Refractive index of particle	1.437	1.433	1.425
Refractive index of solvent	1.490	1.490	1.494
Radius (nm)	47	34.5	23
Stickiness Parameter	1.0	0.9	1.5

Table 2: Parameter Values

The three stearylsilica particle dispersions used by Jansen *et. al.* in his turbidity study were modeled using the multiple scattering theory with adhesive hard spheres. The parameters are given in Table 2, where the values for τ and a are those for best agreement with QCA. The He-Ne laser had a free space wavelength of 632 nm, and the fractional volume of the silica scatterers was varied from $0 - 40\%$.

Figure 15 shows the turbidity as a function of fractional volume for the three particle species, with the stickiness given by the values of τ in Table 2. The results of QCA agree quite well with the experimental data. However, without the assumption of adhesion, the turbidity behavior cannot be explained.

2.3 References

1. S.R. Forrest, and T.A. Witten, "Long-range correlations in smoke particle aggregates," *J. Phys. A: Math. Gen.*, Vol. 12, pp. L109–L117, 1979.

2. R.D. Mountain, G.W. Mulholland, and H. Baum, "Simulations of aerosol agglomeration in the free molecular and continuum flow regimes," *J. Colloid Interf. Sci.*, Vol. 114, pp. 67–81, 1986.

3. R.J. Samson, G.W. Mulholland, and J.W. Gentry, "Structure analysis of soot agglomerates," *Langmuir*, Vol. 3, pp. 272–281, 1987.

4. A.J. Hurd, and W.L. Flower, "In situ growth and structure of fractal silica aggregates in a flame," *J. Colloid Interf. Sci.*, Vol. 122, pp. 178–192, 1988.

5. T.A. Witten, and L.M. Sander, "Diffusion-limited aggregation," *Phys. Rev. B,* Vol. 27, pp. 5686–5697, 1983.

6. P. Meakin, "Formation of fractal clusters and networks by irreversible diffusion-limited aggregation," *Phys. Rev. Lett.,* Vol. 51, pp. 1119–1122, 1983.

7. M. Kolb, R. Botet, and R. Jullien, "Scaling of kinetically grown clusters," *Phys. Rev. Lett.,* Vol. 51, pp. 1123–1126, 1983.

8. R. Botet, R. Jullien, and M. Kolb, "Hierarchical model for irreve kinetic cluster formulation," *J. Phys. A: Math. Gen.,* Vol. 17, pp. L75–L79, 1

9. R. Jullien, and R. Botet, *Aggregation and Fractal Aggregates,* World Scientific, Singapore, 1987.

10. T. Vicsek, *Fractal Growth Phenomena,* World Scientific, Singapore, 1989.

11. B. Peterson, and S. Strom, "T matrix for electromagnetic scattering from an arbitrary number of scatterers and representation of E(3)," *Phys. Rev. D,* Vol. 8, pp. 3661–3678, 1973.

12. L. Tsang, J.A. Kong, and R.T. Shin, *Theory of Microwave Remote Sensing,* Wiley-Interscience, New York, 1985.

13. Charles W. Bruce, Thor F. Stromberg, Kristan P. Gurton, and J.B. Mozer, "Trans-spectral absorption and scattering of electromagnetic radiation by diesel soot," *Appl. Opt.,* Vol. 30, pp. 1537–1546, 1991.

14. L. Tsang, C.E. Mandt, and K.H. Ding, "Monte Carlo simulations of the extinction rate of dense media with randomly distributed dielectric spheres based on solution of Maxwell's equations," *Opt. Lett.,* Vol. 17, pp. 314–316, 1992.

15. O. Edoh, "The Optical Properties of Carbon," Ph.D. Dissertation, University of Arizona, Tucson, 1987.

16. R.J. Baxter, "Percus-Yevick equation for hard spheres with surface adhesion," *J. Chem. Phys.,* Vol 49, pp. 2770–2773, 1968.

17. M.H.G.M. Penders, A. Vrij, "A turbidity study on colloidal silca particles in concentrated suspensions sing the polydisperse adhesive hard sphere model," *J. Chem. Phys.,* Vol. 93, pp. 3704–3711, 1990.

18. P. Dimon, S.K. Sinha, D.A. Weitz, C.R. Safinay, G.S. Smith, W.A. Varady, and H.M. Lindsay, "Structure of Aggregated Gold Colloids," *Phys. Rev. Lett.*, Vo. 57, pp. 595–598, 1986.

19. J.K. Percus, and G.J. Yevick, "Analysis of classical statistical mechanics by means of collective coordinates," *Phys. Rev.*, Vol. 110, pp. 1–13, 1958.

20. R.J. Baxter, "Ornstein-Zernike relation for a disordered fluid," *Aust. J. Phys.*, Vol. 21, pp. 563–569, 1968.

21. B. Barboy, "On a representation of the equation of state of fluids in terms of the adhesive hard-spheres model," *J. Chem. Phys.*, Vol. 61, pp. 3194–3196, 1974.

22. K.H. Ding, C. Mandt, L. Tsang, and J.A. Kong, "Monte Carlo simulations of pair distribution function of dense discrete random media with multiple sizes of particles," *J. of Electro. Waves Applic.*, Vol. 6, pp. 1015–1030, 1992.

23. N.A. Seaton, and E.D. Glandt, "Monte Carlo simulation of adhesive spheres," *J. Chem. Phys.*, Vol. 87, pp. 1785–1790, 1987.

24. W.G.T. Kranendonk, and D. Frenkel, "Simulation of the adhesive-hard-sphere model," *Molec. Phys.*, Vol. 64, pp. 403–424, 1988.

25. K.H. Ding, and L. Tsang, "Effective propagation constants of dense nontenuous media with multi-species of particles," *J. of Electro. Waves Applic.*, Vol. 2, pp. 757–777, 1988.

26. K.H. Ding, and L. Tsang, "Effective propagation constants in media with densely distributed dielectric particles of multiple sizes and permittivities," *Progress in Electromagnetics Research*, Chapter 3, Vol. 1, pp. 241–295, 1989.

27. K.H. Ding, and L. Tsang, "Effective propagation constants and attenuation rates in media of densely distributed coated dielectric particles with size distributions," *J. of Electro. Waves Applic.*, Vol. 5, pp. 117–142, 1991.

28. C.C. Lu, Y.M. Wang, W.C. Chew and L. Tsang, *Proc. of IEEE Antennas and Prop. Symposium*, pp. 1292, 1993.

29. A. Ishimaru, and Y. Kuga, "Attenuation constant of a coherent field in a dense distribution of particles," *J. Opt. Soc. Am.*, Vol. 72, pp. 1317–1320, 1982.

30. J.W. Jansen, C.G. de Kruif, A. Vrij, "Attractions in sterically stabilized silica dispersions II. Experiments on phase separation induced by temperature variation," *J. Colloid Interf. Sci.*, Vol. 114, pp. 481–490, 1986.

3. PUBLICATIONS

K.H. Ding, L. Zurk, and L. Tsang, "Pair Distribution Functions and Attenuation Rates for Sticky Particles in Dense Media," submitted to J. Electro. Waves Applic., 1993.

K.H. Ding, L. Zurk, and L. Tsang, "Pair Distribution Functions and Attenuation Rates for Dense Discrete Random Media with Sticky Particles," Progress In Electromagnetics Research Symposium (PIERS), Pasadena, CA, July 1993.

K.H. Ding, C.E. Mandt, L. Tsang, and J.A. Kong, "Monte Carlo Simulations of Pair Distribution Functions of Particles with Multiple Sizes in Dense Discrete Random Media," J. Electro. Waves Applic., Vol. 6, 1015–1030, 1992.

L. Tsang, C.E. Mandt, and K.H. Ding, "Monte Carlo Simulations of Extinction Rate of Dense Media with Randomly Distributed Dielectric Spheres Based on Solution of Maxwell's Equations," Optics Letters, Vol. 17, 314–316, 1992.

K.H. Ding, "Scattering and Absorption of Electromagnetic Radiation by Random Fractal Clusters of Particles," IEEE AP/URSI International Symposium, Chicago, IL, July 1992.

K.H. Ding, "Light Scattering of Fractal Aerosol Aggregates Using T-Matrix Method," Proceedings SPIE 1688, Atmospheric Propagation and Remote Sensing, Orlando, FL, April 1992, 144–151.

L. Tsang, K.H. Ding, D. Winebrenner, and J.A. Kong, "Scattering of Waves from Dense Discrete Random Media: Theory and Applications in Remote Sensing," Proceedings SPIE 1558, Wave Propagation and Scattering in Varied Media II, San Diego, CA, July 1991, 260–268.

K.H. Ding, C.E. Mandt, L. Tsang, and J.A. Kong, "Monte Carlo Simulations of Pair Distribution Functions of Particles with Multiple Sizes in Dense Discrete Random Media," Progress In Electromagnetics Research Symposium (PIERS), Cambridge, MA, July 1991.

4. PERSONNEL SUPPORTED AND DEGREES AWARDED

Principal Investigator

Kung-Hau Ding

Appendix A

The translational matrix $\overline{\overline{\sigma}}(k\bar{r})$ for vector spherical waves in equation (9) is expressed in the form of [12]

$$\overline{\overline{\sigma}}(k\bar{r}) = \begin{bmatrix} \overline{\overline{A}}(k\bar{r}) & \overline{\overline{B}}(k\bar{r}) \\ \overline{\overline{B}}(k\bar{r}) & \overline{\overline{A}}(k\bar{r}) \end{bmatrix} \tag{A.1}$$

where the matrices $\overline{\overline{A}}(k\bar{r})$ and $\overline{\overline{B}}(k\bar{r})$ are of dimension $L_{max} \times L_{max}$. $L_{max} = N_{max}(N_{max}+2)$ and N_{max} is the maximum order kept in the summation. The expressions of their elements, $A_{\mu\nu mn}(k\bar{r})$ and $B_{\mu\nu mn}(k\bar{r})$, are given as follows.

$$\begin{aligned} A_{\mu\nu mn}(k\bar{r}) &= \frac{\gamma_{mn}}{\gamma_{\mu\nu}}(-1)^{\mu} \sum_{p} a(m,n|-\mu,\nu|p)a(n,\nu,p) \\ &\quad \times h_p(kr)Y_p^{m-\mu}(\theta,\phi) \end{aligned} \tag{A.2}$$

$$\begin{aligned} B_{\mu\nu mn}(k\bar{r}) &= \frac{\gamma_{mn}}{\gamma_{\mu\nu}}(-1)^{\mu+1} \sum_{p} a(m,n|-\mu,\nu|p,p-1)b(n,\nu,p) \\ &\quad \times h_p(kr)Y_p^{m-\mu}(\theta,\phi) \end{aligned} \tag{A.3}$$

where

$$\begin{aligned} a(m,n|\mu,\nu|p) &= (-1)^{m+\mu}(2p+1)\left[\frac{(n+m)!(\nu+\mu)!(p-m-\mu)!}{(n-m)!(\nu-\mu)!(p+m+\mu)!}\right]^{1/2} \\ &\quad \times \begin{pmatrix} n & \nu & p \\ m & \mu & -(m+\mu) \end{pmatrix} \begin{pmatrix} n & \nu & p \\ 0 & 0 & 0 \end{pmatrix} \end{aligned} \tag{A.4}$$

$$\begin{aligned} a(m,n|\mu,\nu|p,q) &= (-1)^{m+\mu}(2p+1)\left[\frac{(n+m)!(\nu+\mu)!(p-m-\mu)!}{(n-m)!(\nu-\mu)!(p+m+\mu)!}\right]^{1/2} \\ &\quad \times \begin{pmatrix} n & \nu & p \\ m & \mu & -(m+\mu) \end{pmatrix} \begin{pmatrix} n & \nu & q \\ 0 & 0 & 0 \end{pmatrix} \end{aligned} \tag{A.5}$$

$$\begin{aligned} a(n,\nu,p) = \frac{i^{\nu-n+p}}{2\nu(\nu+1)} &\left[2\nu(\nu+1)(2\nu+1) + (\nu+1)(n+\nu-p)(n+p-\nu+1) \right. \\ &\left. - \nu(n+\nu+p+2)(\nu+p-n+1)\right]^{1/2} \end{aligned} \tag{A.6}$$

$$\begin{aligned} b(n,\nu,p) = -\frac{(2\nu+1)}{2\nu(\nu+1)} i^{\nu-n+p} &\left[(n+\nu+p+1)(\nu+p-n) \right. \\ &\left. \times (n+p-\nu)(n+\nu-p+1)\right]^{1/2} \end{aligned} \tag{A.7}$$

and

$$\begin{pmatrix} j_1 & j_2 & j_3 \\ m_1 & m_2 & -(m_1+m_2) \end{pmatrix} \tag{A.8}$$

are the Wigner $3j$ symbols, $h_p(kr)$ is spherical Hankel function of first kind of order p, and $Y_n^m(\theta,\phi)$, $Y_n^m(\theta,\phi) = P_n^m(\cos\theta)e^{im\phi}$, is spherical harmonic and $P_n^m(\cos\theta)$, $m = 0, \pm 1, \cdots, \pm n$ are associated Legendre polynomials. Also

$$\gamma_{mn} = \sqrt{\frac{(2n+1)(n-m)!}{4\pi n(n+1)(n+m)!}} \tag{A.9}$$

Appendix B

The vector spherical waves are [12]

$$Rg\overline{M}_{mn}(k\bar{r}) = \gamma_{mn} j_n(kr)\overline{C}_{mn}(\theta,\phi) \tag{B.1}$$

$$Rg\overline{N}_{mn}(k\bar{r}) = \gamma_{mn}\left\{\frac{n(n+1)j_n(kr)}{kr}\overline{P}_{mn}(\theta,\phi) + \frac{[krj_n(kr)]'}{kr}\overline{B}_{mn}(\theta,\phi)\right\} \tag{B.2}$$

where

$$\overline{P}_{mn}(\theta,\phi) = \hat{r}Y_n^m(\theta,\phi) \tag{B.3}$$

$$\overline{B}_{mn}(\theta,\phi) = \left[\hat{\theta}\frac{dP_n^m(\cos\theta)}{d\theta} + \hat{\phi}\frac{im}{\sin\theta}P_n^m(\cos\theta)\right]e^{im\phi} \tag{B.4}$$

$$\overline{C}_{mn}(\theta,\phi) = \left[\hat{\theta}\frac{im}{\sin\theta}P_n^m(\cos\theta) - \hat{\phi}\frac{dP_n^m(\cos\theta)}{d\theta}\right]e^{im\phi} \tag{B.5}$$

are vector spherical harmonics and j_n is spherical Bessel function of order n. In (B1) and (B2), Rg stands for regular part of the wave function. For vector waves $\overline{M}_{mn}(k\bar{r})$ and $\overline{N}_{mn}(k\bar{r})$ without "Rg", they are the same expressions as (B1) and (B2) respectively with j_n replaced by h_n, spherical Hankel function of first kind and of order n.

The T matrix coefficients for a sphere with radius a, permittivity ϵ_s, and wavenumber $k_s = \omega\sqrt{\mu\epsilon_s}$ are

$$T_n^{(M)} = -\frac{j_n(k_sa)[kaj_n(ka)]' - j_n(ka)[k_saj_n(k_sa)]'}{j_n(k_sa)[kah_n(ka)]' - h_n(ka)[k_saj_n(k_sa)]'} \tag{B.6}$$

$$T_n^{(N)} = -\frac{[k_s^2a^2j_n(k_sa)][kaj_n(ka)]' - [k^2a^2j_n(ka)][k_saj_n(k_sa)]'}{[k_s^2a^2j_n(k_sa)][kah_n(ka)]' - [k^2a^2h_n(ka)][k_saj_n(k_sa)]'} \tag{B.7}$$

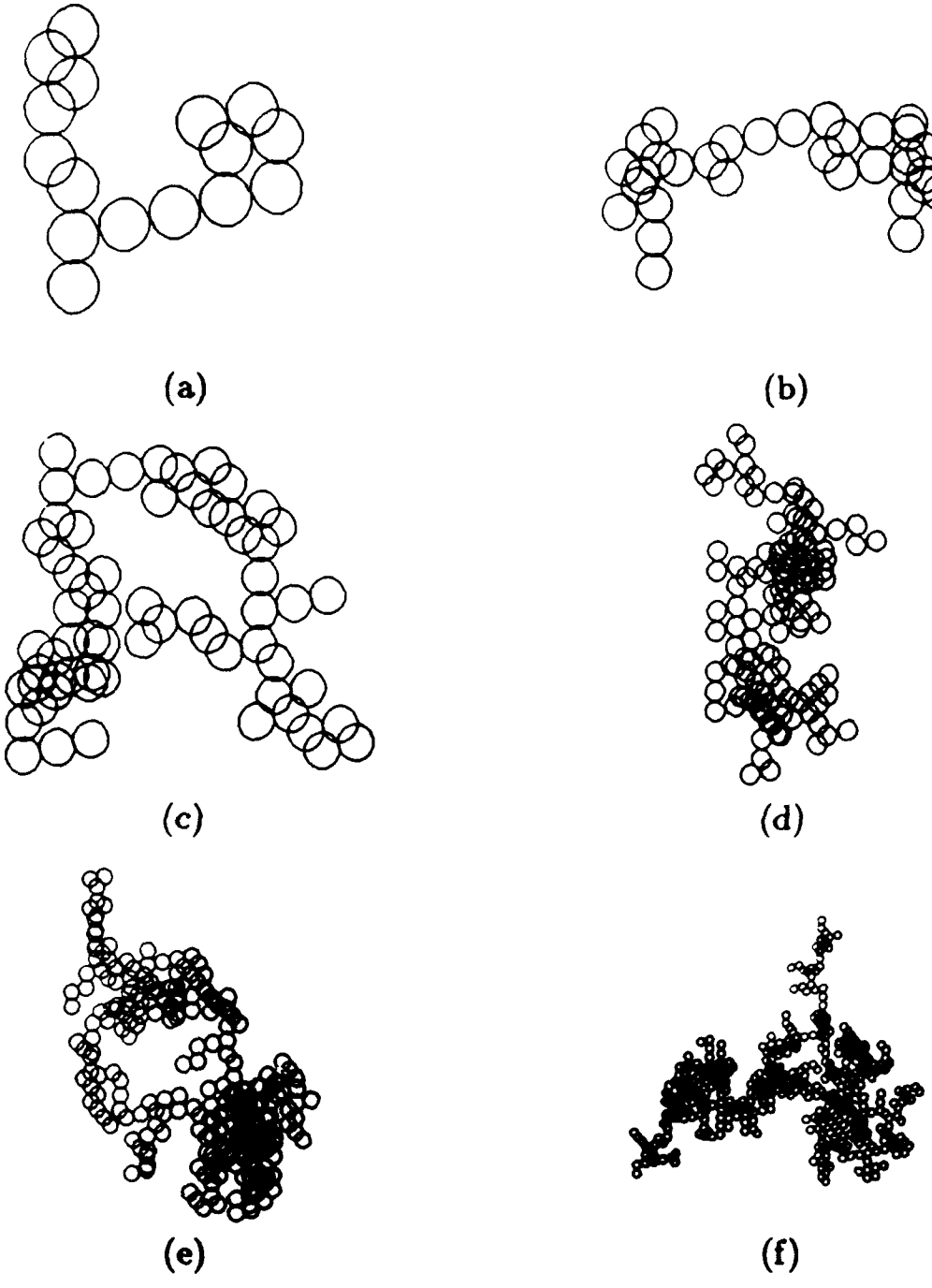

Figure 1. Examples of 3-dimensional aggregates obtained by the hierarchical CCA model, (a) 16 particles; (b) 32 particles; (c) 64 particles; (d) 128 particles; (e) 256 particles; and (f) 512 particles.

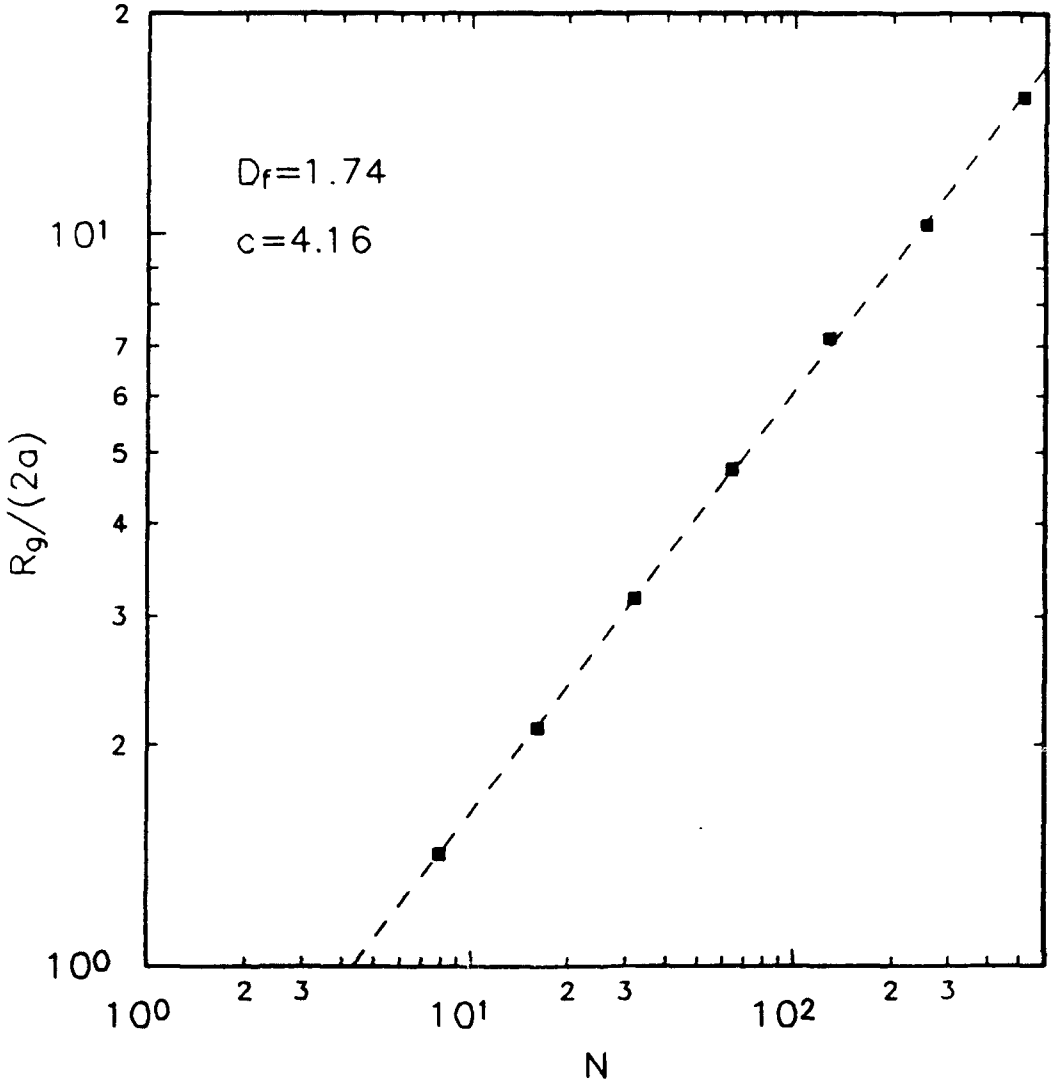

Figure 2. Radius of gyration R_g as a function of the number of spherules N. The squares are results of the hierarchical CCA model.

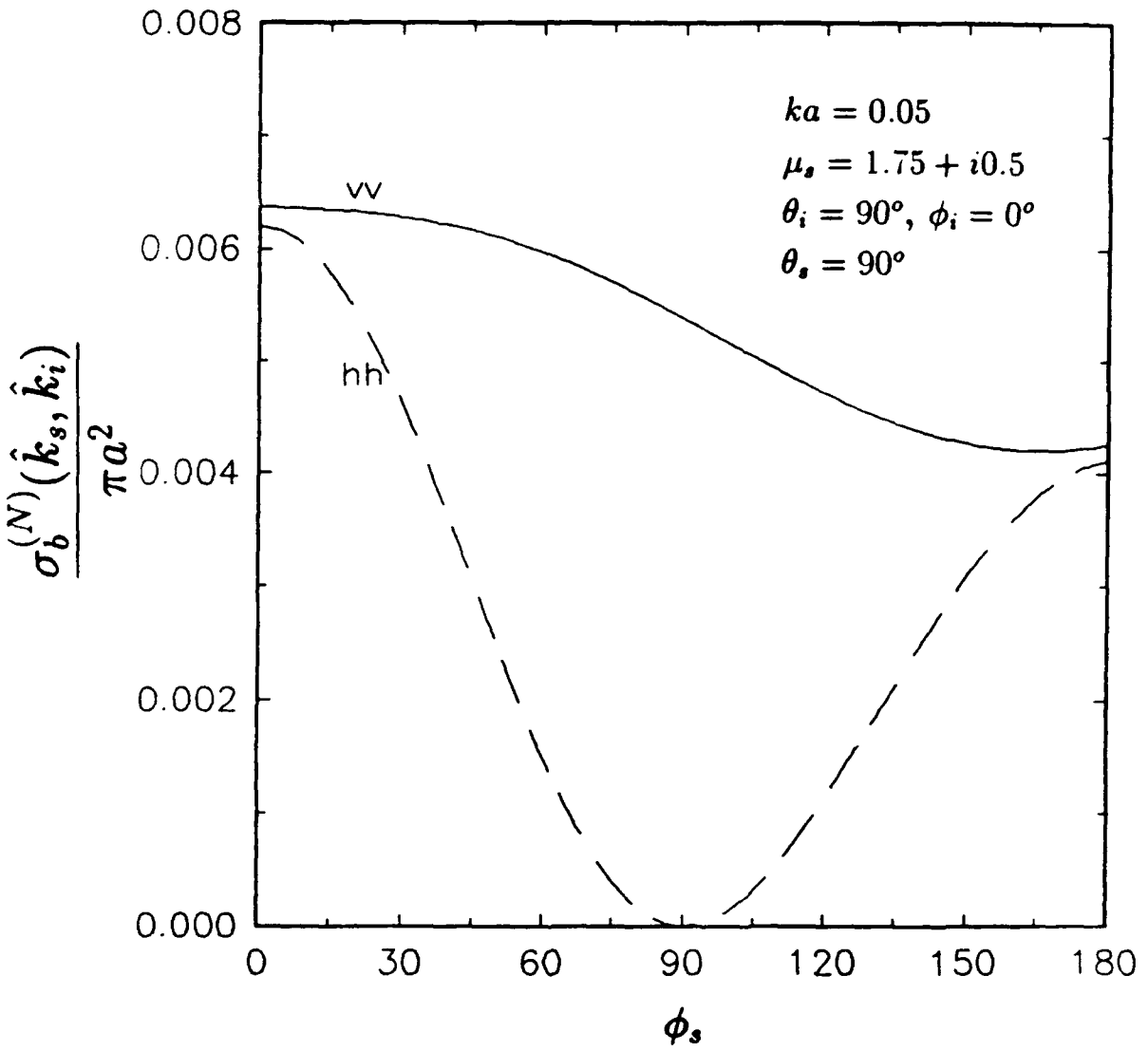

Figure 3(a). Bistatic scattering cross section as a function of ϕ_s for an aggregate with 32 spheres (see Figure 1(b)). Other parameters are $\mu_s = 1.75 + i0.5$, $ka = 0.05$, $\theta_i = 90^o$, $\phi_i = 0^o$ and $\theta_s = 90^o$.

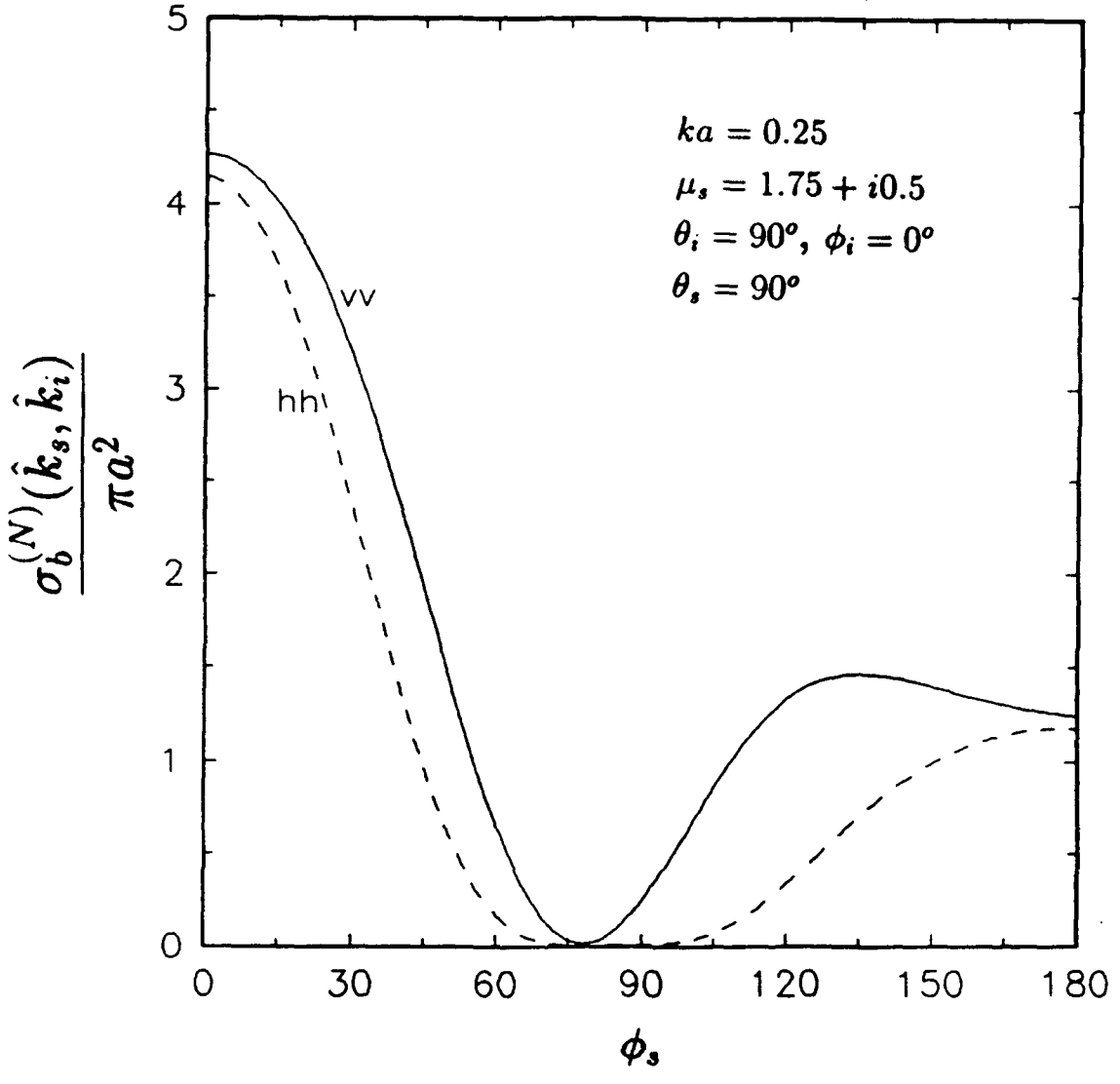

Figure 3(b). Bistatic scattering cross section as a function of ϕ_s for an aggregate with 32 spheres (see Figure 1(b)). Other parameters are $\mu_s = 1.75 + i0.5$, $ka = 0.25$, $\theta_i = 90°$, $\phi_i = 0°$ and $\theta_s = 90°$.

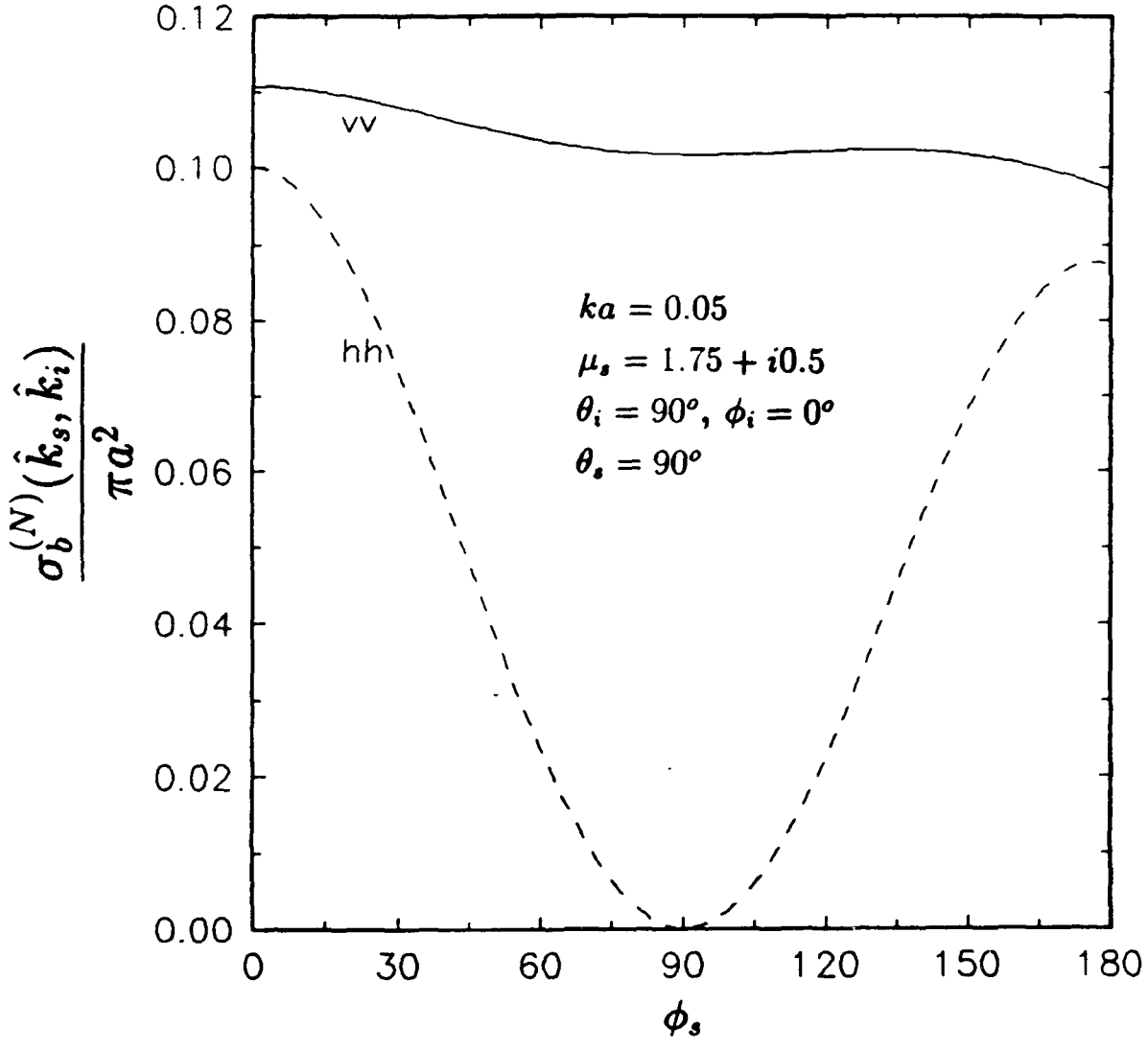

Figure 4(a). Bistatic scattering cross section as a function of ϕ_s for an aggregate with 128 spheres (see Figure 1(d)). Other parameters are $\mu_s = 1.75 + i($ $)$, $ka = 0.05$, $\theta_i = 90°$, $\phi_i = 0°$ and $\theta_s = 90°$.

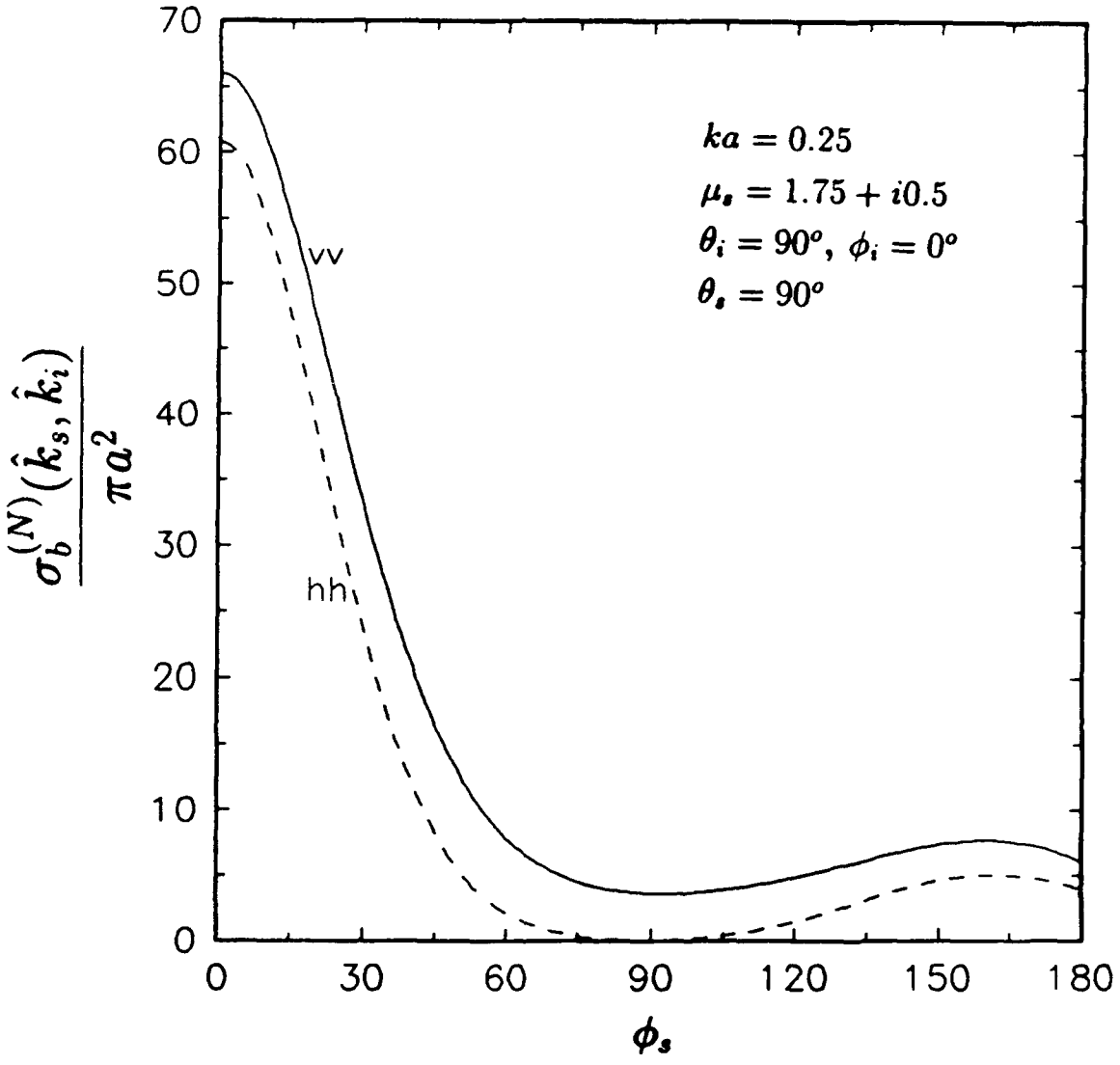

Figure 4(b). Bistatic scattering cross section as a function of ϕ_s for an aggregate with 128 spheres (see Figure 1(d)). Other parameters are $\mu_s = 1.75 + i0.5$, $ka = 0.25$, $\theta_i = 90°$, $\phi_i = 0°$ and $\theta_s = 90°$.

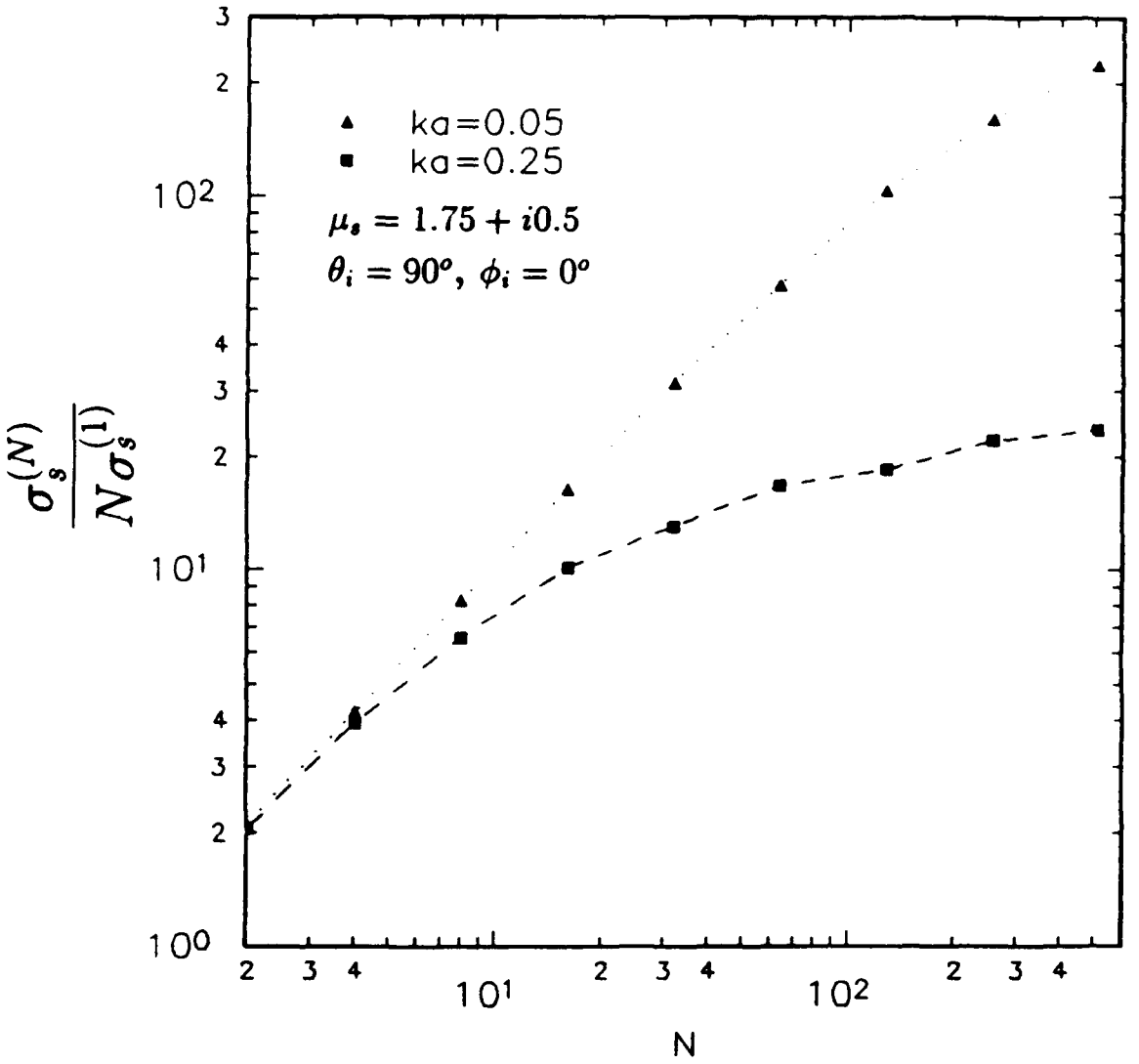

Figure 5. Scattering cross section as a function of number of primary particles within a cluster. Other parameters are $\mu_s = 1.75 + i0.5$, $ka = 0.05, \text{and} 0.25$, $\theta_i = 90°$, and $\phi_i = 0°$.

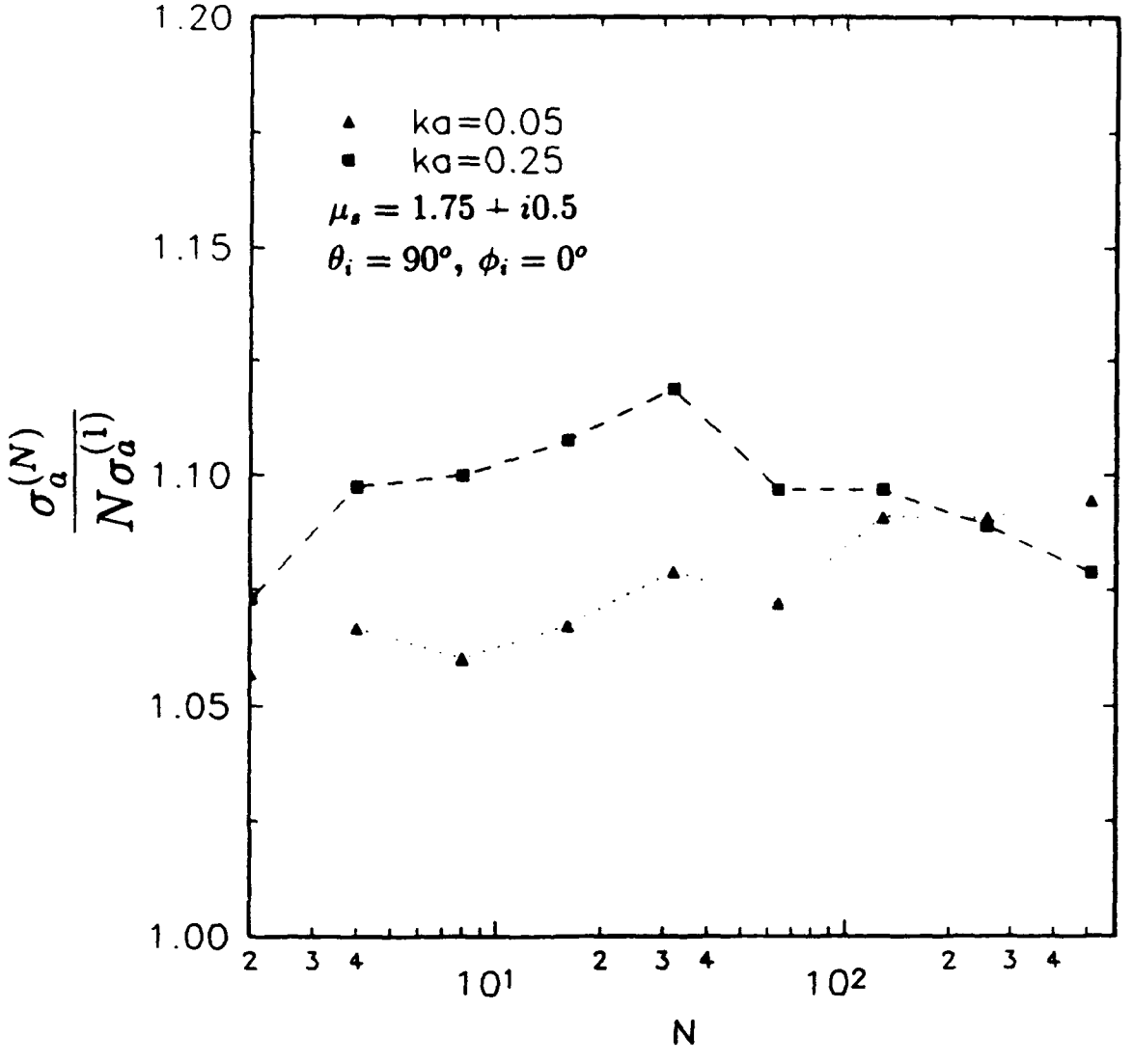

Figure 6. Absorption cross section as a function of number of primary particles within a cluster. Other parameters are $\mu_s = 1.75 + i0.5$, $ka = 0.05, \text{and} 0.25$, $\theta_i = 90°$, and $\phi_i = 0°$.

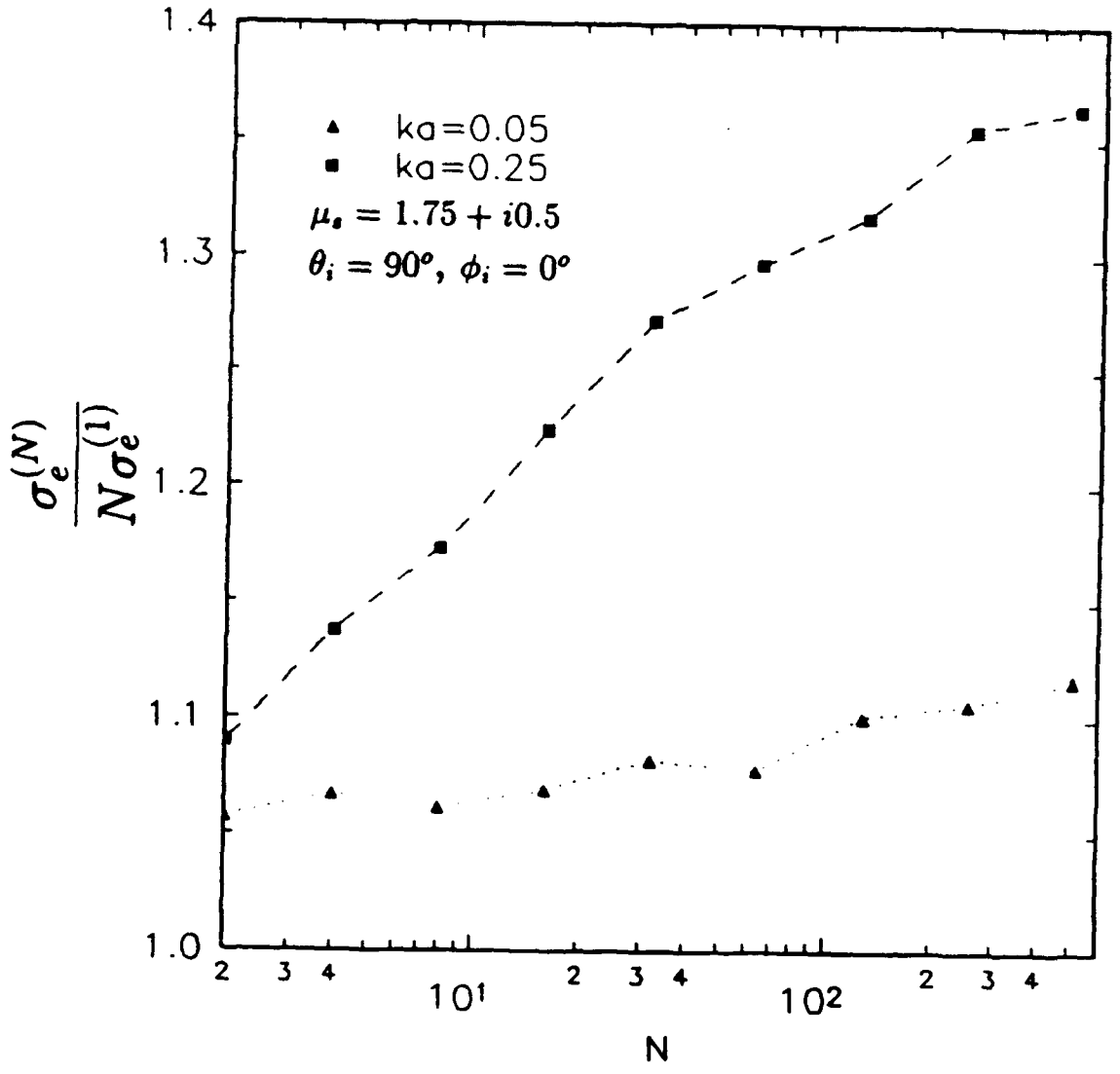

Figure 7. Extinction cross section as a function of number of primary particles within a cluster. Other parameters are $\mu_s = 1.75 + i0.5$, $ka = 0.05, \text{and} 0.25$, $\theta_i = 90°$, and $\phi_i = 0°$.

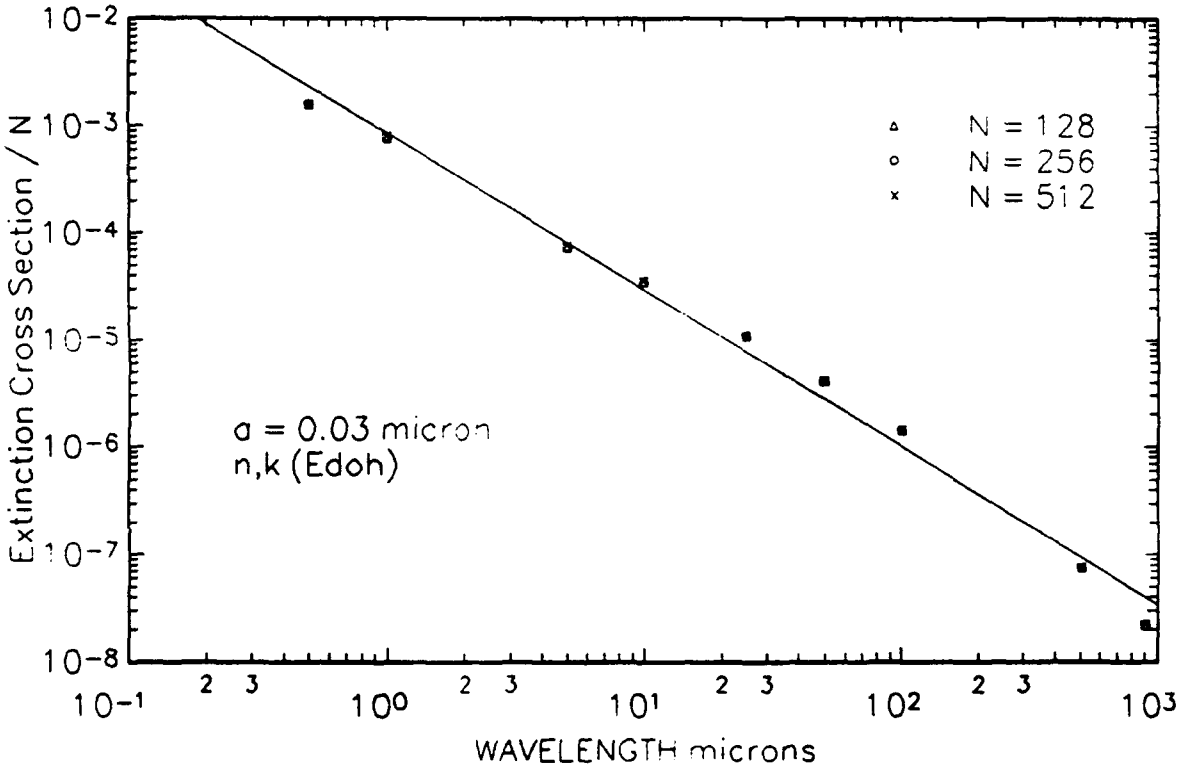

Figure 8. Extinction cross section per constituent particle as a function of wavelength. The number of particles in an aggregate are $N = 128, 256, \text{and} 512$. The radius of sphere is $a = 0.03 \mu m$.

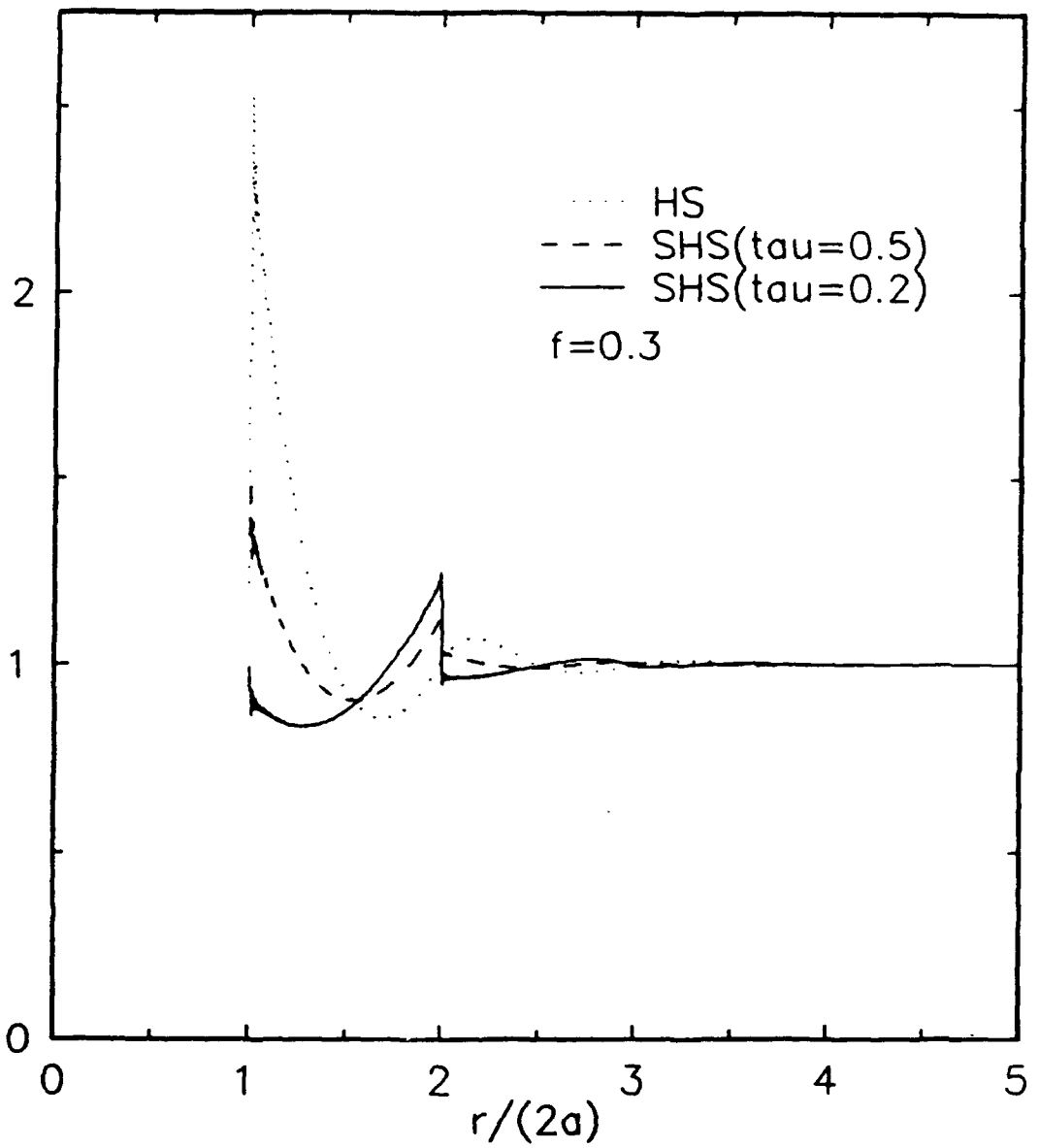

Figure 9. Percus-Yevick Pair distribution function for sticky spheres with $\tau = 0.2$ and $\tau = 0.5$, and for non-sticky spheres.

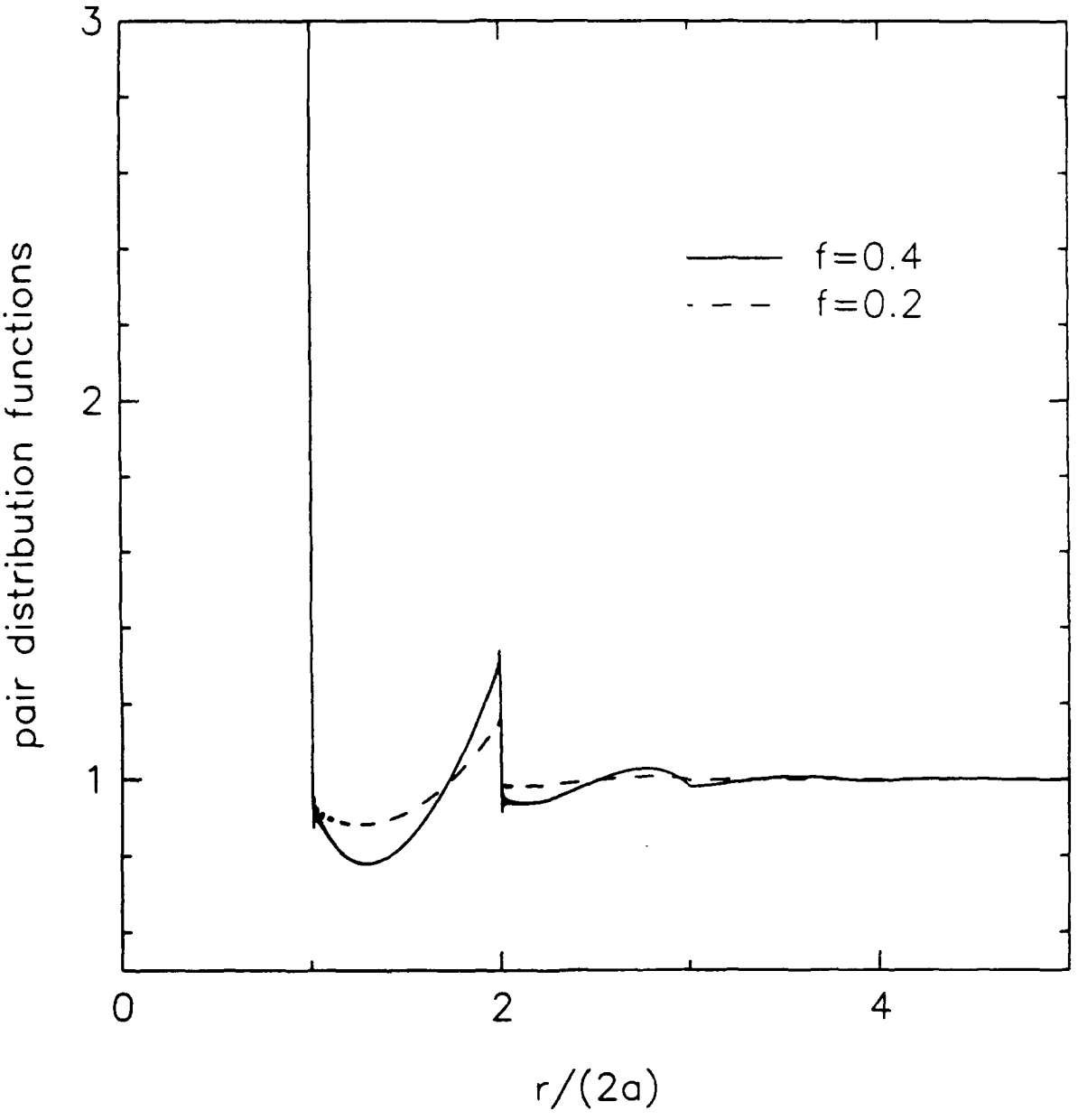

Figure 10. Percus-Yevick Pair distribution function for sticky spheres with $f = 0.2$ and $f = 0.4$ and stickiness $\tau = 0.2$.

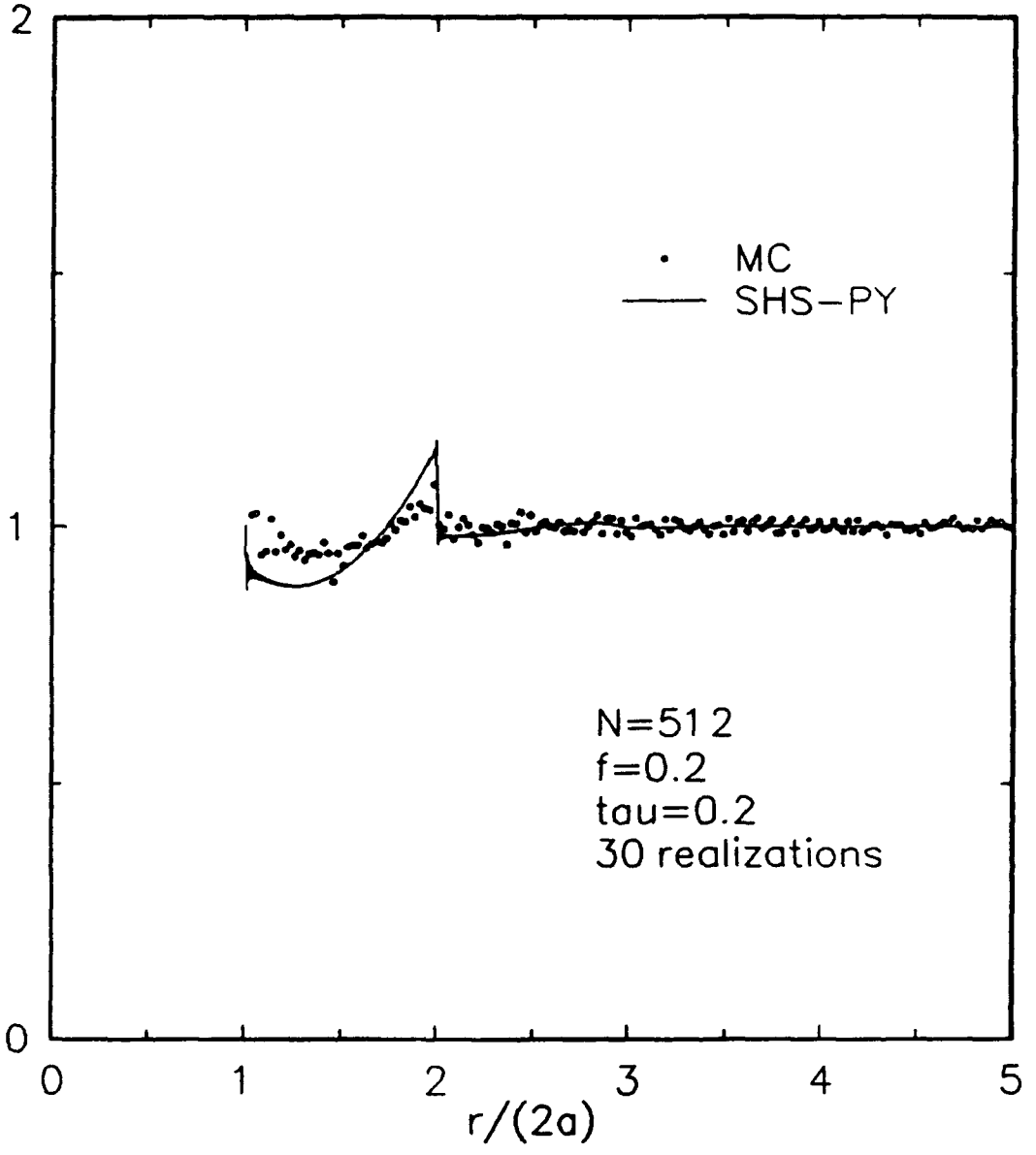

Figure 11. Pair distribution function for media with sticky spheres. The simulation parameters are $f = 0.2$, $\tau = 0.2$, $N = 512$, and 30 realizations. The simulated results are compared with Percus-Yevick calculations.

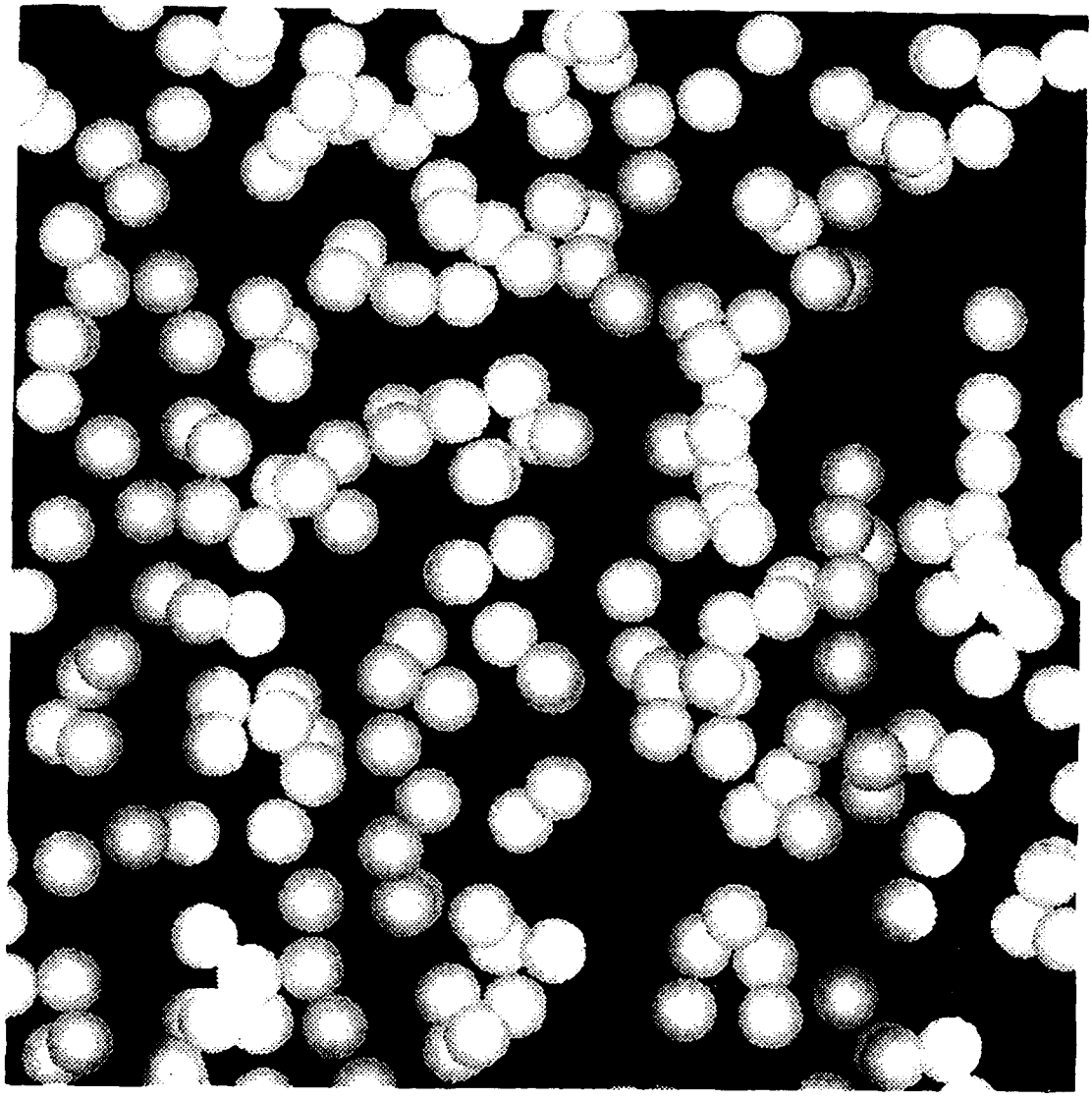

Figure 12. A typical configuration for media with sticky spheres at $f = 0.2$ and $\tau = 0.2$.

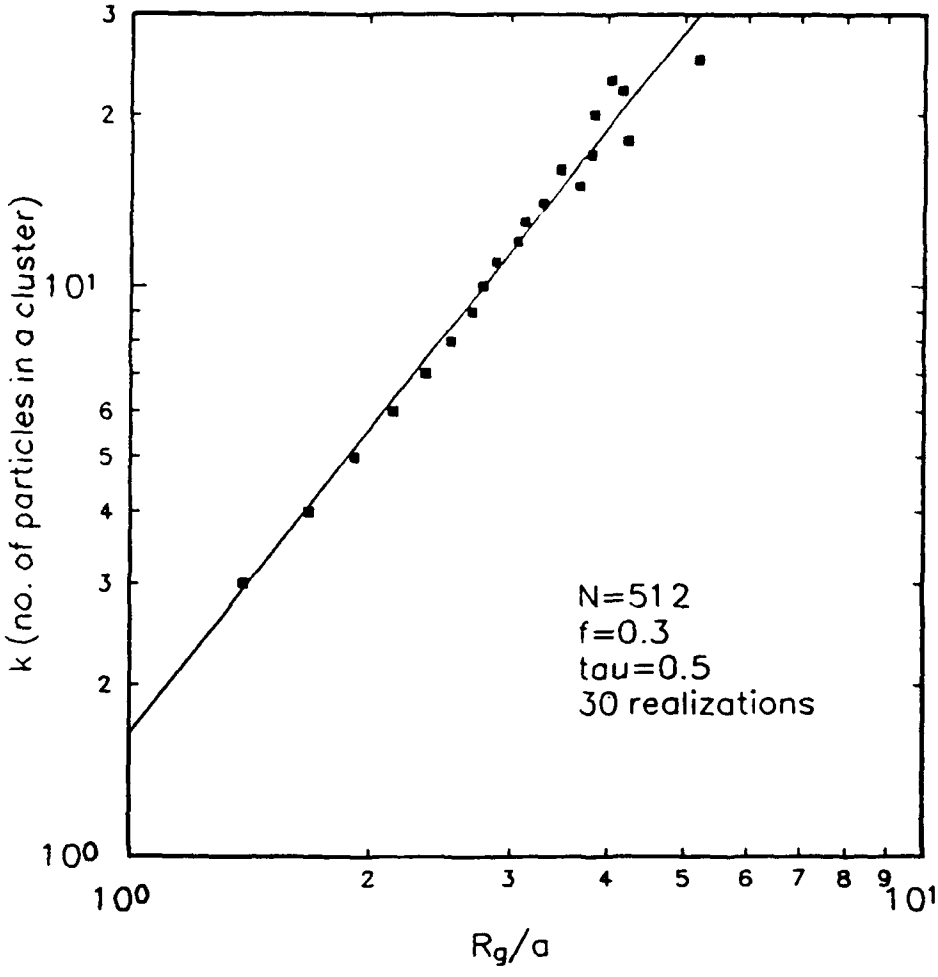

Figure 13. Radius of gyration R_g as a function of the number of spherules N. The squares are results of the SHS model.

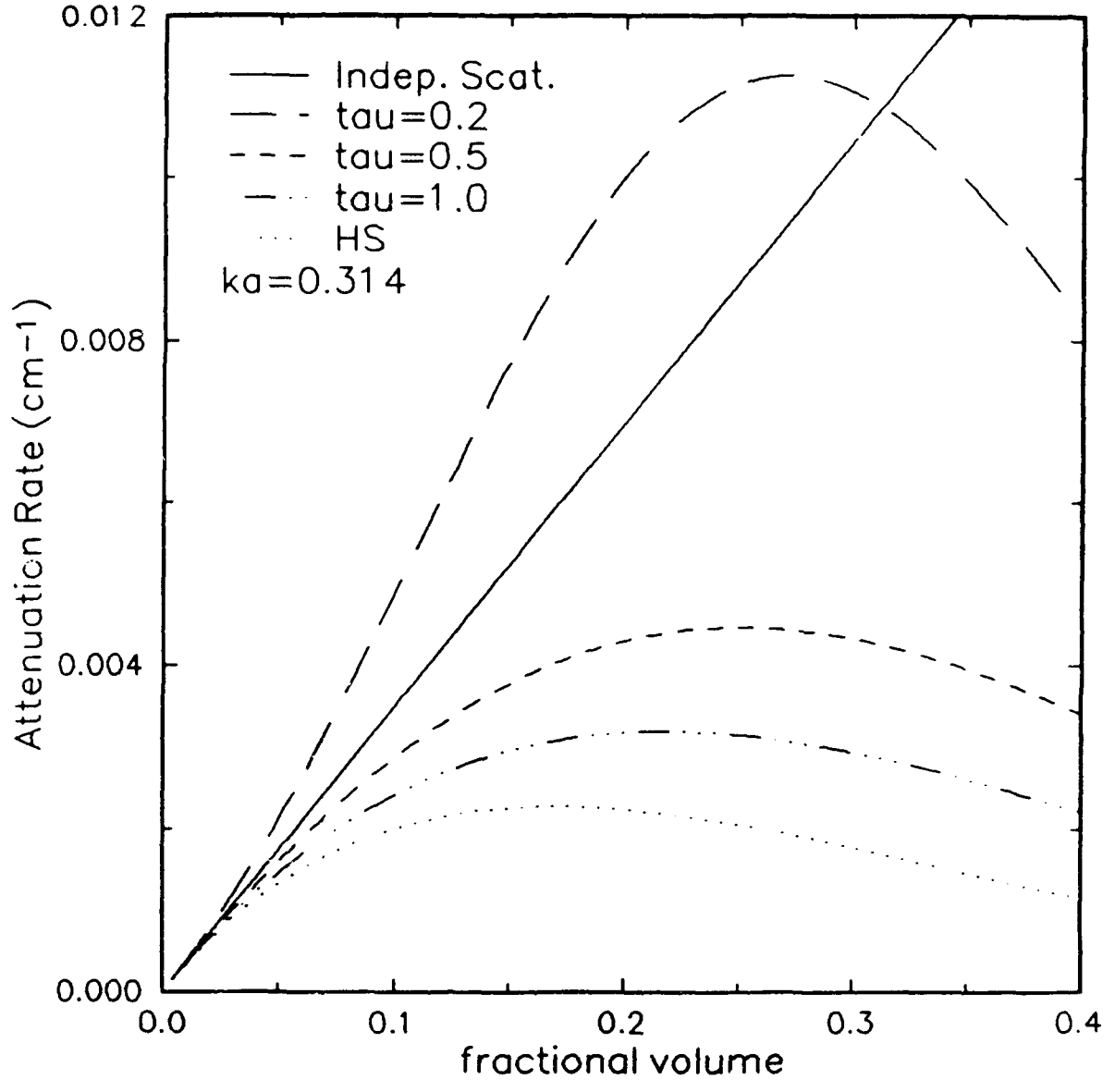

Figure 14. Attenuation rates based on QCA-CP and independent scattering as a function of fractional volume for various stickiness parameters. Other parameters are $\epsilon_s = 3.2\epsilon_o$ and $ka = 0.314$.

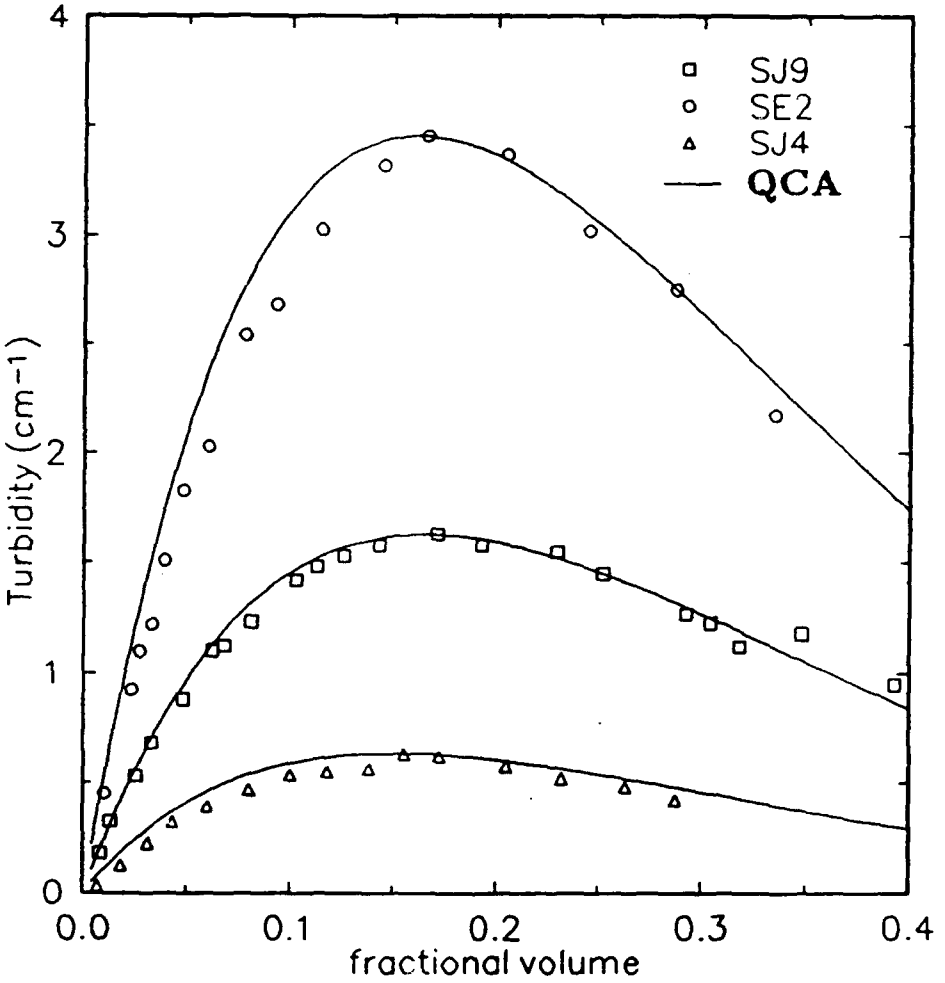

Figure 15. Turbidity as a function of fractional volume calculated with the parameters in Table 2 using QCA-SHS.